



Global Fréchet regression from time correlated bivariate curve data in manifolds

A. Torres-Signes¹ · M. P. Frías² · M. D. Ruiz-Medina³ 

Received: 7 April 2023 / Revised: 12 February 2025 / Published online: 4 April 2025
© The Author(s) 2025

Abstract

Global Fréchet regression is addressed from the observation of a strictly stationary bivariate curve process, evaluated in a finite-dimensional compact differentiable Riemannian manifold with bounded positive smooth sectional curvature. The involved univariate curve processes respectively define the functional response and regressor, having the same Fréchet functional mean. The supports of the marginal probability measures of the regressor and response processes are assumed to be contained in a ball, whose radius ensures the injectivity of the exponential map. This map has a time-varying origin at the common marginal Fréchet functional mean. A weighted Fréchet mean approach is adopted in the definition of the theoretical loss function. The regularized Fréchet weights are computed in the time-varying tangent space from the log-mapped regressors. Under these assumptions, and some Lipschitz regularity sample path conditions, when a unique minimizer exists, the uniform weak-consistency of the empirical Fréchet curve predictor is obtained, under mean-square ergodicity of the log-mapped regressor process in the first two moments. A simulated example in the sphere illustrates the finite sample size performance of the proposed Fréchet predictor. Predictions in time of the spherical coordinates of the magnetic field vector are obtained from the time-varying geocentric latitude and longitude of the satellite NASA's MAGSAT spacecraft in the real-data example analyzed.

Keywords Fréchet functional regression · Riemannian manifold · Time correlated manifold-valued bivariate curve data · Weak-consistency

✉ M. D. Ruiz-Medina
mruiz@ugr.es

A. Torres-Signes
a.torres@uma.es

M. P. Frías
mpfrías@ujaen.es

¹ University of Málaga, Málaga, Spain

² University of Jaén, Jaén, Spain

³ University of Granada, Granada, Spain

1 Introduction

Nonparametric regression techniques have been widely applied in the last few decades to solve prediction problems from data lying on a Riemannian manifold [see Bhattacharya and Bhattacharya (2012)]. Special attention has been paid to kernel estimation, and local polynomial regression exploiting the local character of the exponential map. In the context of manifold-valued response and Euclidean predictors, external local regression embeds the manifold where the response lies onto a higher dimensional Euclidean space, obtaining a local regression estimate in that space, and back to the manifold via a homeomorphism relating the corresponding tangent spaces [(see, e.g., Lin et al. (2017)]. In the same context of manifold-valued response and Euclidean regressors, in Zhu et al. (2009), an intrinsic regression model for the analysis of positive definite matrices is proposed for medical imaging processing. It is well-known that positive definite matrices do not form a vector space. For these random elements in Riemannian manifolds, a semiparametric regression model is proposed, considering a link function to map from the Euclidean space of covariates to the Riemannian manifold of positive definite matrices (see also approaches introduced in Bhattacharya and Bhattacharya (2012); Di Marzio et al. (2014); Khardani and Yao (2022); Kim and Park (2013); Patrangenaru and Ellingson (2016); Pelletier (2005, 2006), mainly from a nonparametric statistical framework).

Different versions of Functional Principal Component Analysis on manifolds have been derived motivated by several fields of applications. An intrinsic principal component analysis of Riemannian manifold-valued functional data, the so-called Riemannian Functional Principal Component Analysis (RFPCA), is obtained in Dai and Müller (2018). We also refer to the nonlinear manifold representation of L^2 random functions themselves, lying in a low-dimensional but unknown manifold, or to the consideration of functional predictors lying on a smooth low-dimensional manifold (see Chen and Müller (2012); Dimeglio et al. (2014); Lazar and Lin (2017); Lin and Yao (2017)).

Among other fields of application, the presented Fréchet functional regression approach in finite-dimensional compact Riemannian manifolds is of interest, for example, in the analysis of bivariate plain trajectory data (see Dai and Müller (2018) where RFPC is applied); prediction from movement data in a pandemic (see Torres-Signes et al. (2021) for the Euclidean setting); prediction of wind directions in environmental risk assessment (see Sect. 9.2 in Di Marzio et al. (2014)); prediction of uniform deviations of comet orbits [see, e.g., Jupp et al. (2003)] [see also Pigoli et al. (2016) on kriging techniques for manifold-valued random fields]. Another field of application where the statistical analysis of manifold data, beyond the sphere, plays a crucial role is brain imaging data. For example, in the detection of brain diseases or disorders, the statistical analysis of covariates providing information about the brain structural and morphological characteristics of individuals plays a crucial role in the construction of RAVENS maps reflecting local volumetric group differences [see, e.g., Zhou et al. (2013); Zhu et al. (2009)]. In this paper, in the real-data example analyzed in Sect. 6, we illustrate the performance of the proposed Fréchet functional regression approach, in the prediction of the time-varying spherical coordinates of the magnetic field vector

from the geocentric latitude and longitude of the satellite NASA's MAGSAT spacecraft, extending the purely spatial analysis of Di Marzio et al. (2014).

To the best of our knowledge, no systematic approach or theoretical analysis has been developed, in the context of global intrinsic regression in manifolds from time correlated bivariate curve data. This issue has been addressed in the present paper adopting the theoretical framework of bivariate curve processes with values in a compact finite-dimensional Riemannian manifold, displaying suitable geometrical characteristics [see conditions (i)–(ii) in Sect. 3.1 below]. Our proposal is based on the weighted Fréchet mean approach formulated in Petersen and Müller (2019) for Euclidean regressors, and response evaluated in a metric space. Specifically, we extend this formulation to the context of infinite-dimensional response and regressors, correlated in time, and evaluated in a finite-dimensional compact Riemannian manifold. One of the main difficulties arising in addressing this extended formulation is related to the uniform continuity of the theoretical predictor, as well as of its empirical version in probability, both characteristics ensuring uniform weak-consistency. In particular, mean-square first-order and second-order ergodicity of the log-mapped regressor in the time-varying tangent space is assumed in Sect. 3.1 for proving the weak-consistency of the empirical loss function. Fréchet weights are computed in a regularized version of the ambient Hilbert space \mathbb{H} in the time-varying tangent space, in terms of the semi-inner product of the Reproducing Kernel Hilbert Space (RKHS) of the log-mapped regressor process [see, e.g., Galeano et al. (2015); Ruiz-Medina and Álvarez-Liébana (2019); Kuelbs (1970)]. The involved regularizer matrix operator is defined from the pure point spectral properties of the matrix autocovariance operator of the log-mapped regressors in Sect. 3.2.

Among some additional geometrical and sample path Lipschitz regularity conditions, another challenging topic to be addressed in our work is the existence and uniqueness of the Fréchet functional predictor, that requires some probabilistic structural restrictions on the underlying bivariate curve process. Specifically, strictly stationarity of this process is assumed. The inclusion on a closed ball of the support of the marginal infinite-dimensional probability measures of the response and regressor processes is also assumed, ensuring injectivity of the exponential maps, with time-varying origin at the Fréchet functional mean, that minimizes the quadratic mean geodesic dispersion of the curve values of the regressor and response processes. An extensive literature exists on the existence and uniqueness of the global L^p center of mass (minimizer of the L^p -energy function) of an arbitrary probability measure on a manifold. This topic has been addressed, in particular, for complete and connected Riemannian manifolds, under some compactness assumptions on the support of the underlying probability measure [see, e.g., Theorem 2.1 in Afsari (2011) and Buss and Fillmore (2001)]. Specifically, if the support of the probability measure is contained in a ball, whose radius is bounded by a function of p , the injectivity radius of the manifold, and an upper bound on the manifold sectional curvatures, existence and uniqueness hold. Convexity is a notion that plays a crucial role in this problem [see, e.g., the overview presented in Sect. 1.1 in Afsari (2011)]. In Afsari et al. (2013), the convergence of a constant step-size gradient descent algorithm is also investigated for solving this problem, in a general manifold context, analyzing the effect of the curvature and topology of the manifold on the behavior of the algorithm. Beyond the

above geometrical restrictions on the Riemannian manifold, we refer to the reader to Theorem 1 in Le and Barden (2014). As commented, in this paper, we pay attention to the L^2 center of mass of a probability measure defining its Fréchet mean. The values of our Fréchet curve predictor can be identified with the respective L^2 centers of mass of a family of probability measures indexed by the curve arguments of this predictor.

The performance of the proposed Fréchet functional regression methodology is illustrated through simulations in a numerical example in the sphere in \mathbb{R}^3 . The implemented simulation algorithm is based on the generation of the curve values of the regressor process by subordination, via the poinwise application of the inverse von Mises-Fisher distribution transform, to a family of correlated vector diffusion processes, whose sample paths are mapped into the unit ball of the three dimensional Euclidean space. The curve response process is then generated in the time-varying tangent space, by applying a bounded correlation operator to the log-mapped regressor curve values, and adding a strong Gaussian white noise process, generated from the Karhunen–Loéve expansion. These simulations show a good finite sample size performance of our Fréchet functional regression predictor.

In the real-data example analyzed in the context of world magnetic models, 5-fold cross validation is implemented for testing the quality of our Fréchet functional predictions of the time-varying spherical coordinates of the magnetic field vector, from the geocentric latitude and longitude of the satellite NASA's MAGSAT spacecraft. Data have been obtained from NASA's National Space Science Data Center, in the period 02/11/1979–06/05/1980. They have been recorded every half second, and correspond to the first satellite NASA's MAGSAT spacecraft, which orbited the earth every 88 min during seven months at around 400 km altitude.

The outline of the paper is the following. Some preliminaries on Riemannian manifolds and Fréchet regression are given in Sect. 2. Section 3 introduces the assumed conditions, and the proposed regression methodology from manifold-valued bivariate curve data correlated in time. Under suitable conditions, the uniform weak-consistency of the empirical Fréchet functional regression predictor is derived in Theorem 1 of Sect. 4. The proof of this result is given in Appendix A. Simulations in Sect. 5 illustrate the finite sample size performance of the proposed manifold Fréchet functional regression predictor. The performance of this predictor is also analyzed from a real data example in Sect. 6. Appendix B complements the sample information and cross validation results displayed in Sect. 6. Final comments are summarized in Sect. 7.

2 Preliminaries

Let \mathcal{M} be a smooth manifold with topological dimension d in a Euclidean space \mathbb{R}^{d_0} , $d \leq d_0$. Denote by $\{\mathcal{T}_p\mathcal{M}, p \in \mathcal{M}\}$ the tangent spaces at the points of \mathcal{M} . A *Riemannian metric* on \mathcal{M} is a family of inner products $\mathcal{G}(p) : \mathcal{T}_p\mathcal{M} \times \mathcal{T}_p\mathcal{M} \rightarrow \mathbb{R}$ that smoothly varies over $p \in \mathcal{M}$. Endowed with this Riemannian metric, $(\mathcal{M}, \mathcal{G})$ is a Riemannian manifold. The metric on \mathcal{M} induced by \mathcal{G} is the geodesic distance $d_{\mathcal{M}}$.

The *exponential map* $\exp_p(v)$ is defined for $v \in \mathcal{T}_p\mathcal{M}$, and for each $p \in \mathcal{M}$, in terms of a locally length minimizing curve $\gamma_v = \{\exp_p(tv), t \in [0, 1]\}$, called

geodesic, such that for every $v \in \mathcal{T}_p\mathcal{M}$, $\exp_p(v) = \gamma_v(1)$, where $v \in \mathcal{T}_p\mathcal{M}$. That is, γ_v is the unique geodesic with initial location $\gamma_v(0) = p$, and velocity $\gamma'_v(0) = v$. The inverse of the exponential map is called the *logarithm map*, and is denoted by \log_p , $p \in \mathcal{M}$. The *radius of injectivity* inj_p at a point p of the manifold is the radius of the largest ball about the origin of the tangent space $\mathcal{T}_p\mathcal{M}$ on which \exp_p is a diffeomorphism, for each $p \in \mathcal{M}$. If $(\mathcal{M}, d_{\mathcal{M}})$ is a complete metric space, then \exp_p is defined on the entire tangent space, and \exp_p is a diffeomorphism at a neighborhood of the origin of $\mathcal{T}_p\mathcal{M}$ [see, e.g., Chavel (2006)].

We now briefly introduce the basic probabilistic and function elements involved in the formulation of our approach (see Sect. 3 on the conditions assumed). Denote by $(\Lambda, \mathcal{A}, \mathcal{P})$ the basic probability space. Consider the space $(\mathcal{C}_{\mathcal{M}}(\mathcal{T}), d_{\mathcal{C}_{\mathcal{M}}(\mathcal{T})}) = \{x : \mathcal{T} \rightarrow \mathcal{M} : x \in \mathcal{C}(\mathcal{T})\}$, constituted by \mathcal{M} -valued continuous functions on a compact interval \mathcal{T} with the supremum geodesic distance

$$d_{\mathcal{C}_{\mathcal{M}}(\mathcal{T})}(x(\cdot), y(\cdot)) = \sup_{t \in \mathcal{T}} d_{\mathcal{M}}(x(t), y(t)), \quad \forall x(t), y(t) \in (\mathcal{C}_{\mathcal{M}}(\mathcal{T}), d_{\mathcal{C}_{\mathcal{M}}(\mathcal{T})}).$$

Let $Z = \{Z_s, s \in \mathbb{Z}\}$ be a family of random elements in $(\mathcal{C}_{\mathcal{M}}(\mathcal{T}), d_{\mathcal{C}_{\mathcal{M}}(\mathcal{T})})$ indexed by \mathbb{Z} . Specifically, $Z : \mathbb{Z} \times (\Lambda, \mathcal{A}, \mathcal{P}) \rightarrow \mathcal{C}_{\mathcal{M}}(\mathcal{T})$, and $\mathcal{P}(\omega \in \Lambda; Z_s(\cdot, \omega) \in (\mathcal{C}_{\mathcal{M}}(\mathcal{T}), d_{\mathcal{C}_{\mathcal{M}}(\mathcal{T})})) = 1$, for every $s \in \mathbb{Z}$. Here, $Z_s(t)$ denotes the pointwise value at $t \in \mathcal{T}$ of the curve Z_s in \mathcal{M} , for each $s \in \mathbb{Z}$. Consider the ambient Hilbert space \mathbb{H} of square-integrable vector functions given by

$$\mathbb{H} = \left\{ h(\cdot) = (h_1(\cdot), \dots, h_{d_0}(\cdot))^T : \mathcal{T} \rightarrow \mathbb{R}^{d_0} : \int_{\mathcal{T}} h(t)^T h(t) dt < \infty \right\}. \quad (2.1)$$

This space is equipped with the inner product $\langle h, f \rangle_{\mathbb{H}} = \int_{\mathcal{T}} h(t)^T f(t) dt$, and norm $\|h\|_{\mathbb{H}} = [\langle h, h \rangle_{\mathbb{H}}]^{1/2}$, for any $h, f \in \mathbb{H}$.

For each $s \in \mathbb{Z}$, define the functional (curve) Fréchet mean $\mu_{Z_s, \mathcal{M}}$ as

$$\begin{aligned} \mu_{Z_s, \mathcal{M}}(t) &= \arg \min_{p \in \mathcal{M}} E \left([d_{\mathcal{M}}(Z_s(t), p)]^2 \right) \\ &= \arg \min_{p \in \mathcal{M}} \int_{\mathcal{C}_{\mathcal{M}}(\mathcal{T})} [d_{\mathcal{M}}(z_s(t), p)]^2 dP_{Z_s(t)}(z_s(t)), \quad t \in \mathcal{T}, \end{aligned} \quad (2.2)$$

where $dP_{Z_s(t)}$ denotes the probability measure induced by $Z_s(t)$, the t -projection of the infinite-dimensional marginal probability measure dP_{Z_s} of Z_s , for each $s \in \mathbb{Z}$. Thus, $\mu_{Z_s, \mathcal{M}}$ is the curve in \mathcal{M} providing the best pointwise approximation of Z_s in the mean quadratic geodesic distance sense. The sample path continuity of $Z_s \in (\mathcal{C}_{\mathcal{M}}(\mathcal{T}), d_{\mathcal{C}_{\mathcal{M}}(\mathcal{T})})$ allows the following equivalent definition of the continuous function $\mu_{Z_s, \mathcal{M}}(t)$:

$$\begin{aligned} \mu_{Z_s, \mathcal{M}}(\cdot) &= \arg \min_{z(\cdot) \in \mathcal{C}_{\mathcal{M}}(\mathcal{T})} E \left(\int_{\mathcal{T}} [d_{\mathcal{M}}(Z_s(t), z(t))]^2 dt \right) \\ &= \arg \min_{z(\cdot) \in \mathcal{C}_{\mathcal{M}}(\mathcal{T})} \int_{\mathcal{C}_{\mathcal{M}}(\mathcal{T})} \int_{\mathcal{T}} [d_{\mathcal{M}}(z_s(t), z(t))]^2 dt dP_{Z_s}(z_s). \end{aligned} \quad (2.3)$$

The response $Y = \{Y_s, s \in \mathbb{Z}\}$ and regressor $X = \{X_s, s \in \mathbb{Z}\}$ curve processes are introduced in Sect. 3, under the above scenario, that is, X , and Y satisfy the conditions of process Z .

2.1 Fréchet regression in metric spaces with finite-dimensional Euclidean regressors

This section reviews some material from Petersen and Müller (2019) to motivate the regression approach presented. Let (Ω, d_Ω) be a metric space. Consider a random vector $(X, Y) \sim F$, where $dF(x, y)$ is the probability measure induced by (X, Y) , with X and Y respectively taking values in \mathbb{R}^p and Ω . The marginal distributions of X and Y are denoted as F_X and F_Y , respectively. Assume that the mean vector $\mu_X = E(X)$, and the variance-covariance matrix Σ of the regressors X , as well as the conditional distributions $F_{X|Y}$ and $F_{Y|X}$ exist (see, e.g., Chapter V in Parthasarathy (1967)).

Definition 1 The Fréchet regression predictor $m_\oplus(x)$ of Y given the observed value, $X = x \in \mathbb{R}^p$, is defined as follows:

$$\begin{aligned} m_\oplus(x) &= \arg \min_{\omega \in \Omega} M_\oplus(\omega, x) = \arg \min_{\omega \in \Omega} E(d_\Omega^2(Y, \omega) \mid X = x) \\ &= \arg \min_{\omega \in \Omega} \int_\Omega d_\Omega^2(y, \omega) dF_{Y|X}(x, y). \end{aligned} \tag{2.4}$$

Let us consider the case of real-valued response, i.e., $\Omega = \mathbb{R}$, and $d_\Omega = d_E$, where $d_E(y_1, y_2) = |y_1 - y_2|$. It is well-known that the least-squares linear global regression predictor $m_L(x)$ is computed in a parametric framework from the minimizer

$$(\beta_0^*, \beta_1^*) = \arg \min_{\beta_0 \in \mathbb{R}, \beta_1 \in \mathbb{R}^p} \int \left[\int y dF_{Y|X}(x, y) - (\beta_0 + \beta_1^T(x - \mu_X)) \right]^2 dF_X(x), \tag{2.5}$$

with $E[X] = \mu_X \in \mathbb{R}^p$, where now $dF_{Y|X}(x, y)$ denotes the conditional probability measure on \mathbb{R} induced by Y given $X_{p \times 1} = x_{p \times 1} \in \mathbb{R}^p$, and, as before, $dF_X(x)$ denotes the marginal probability measure on \mathbb{R}^p induced by X . It is well-known that the scalar intercept $\beta_0^* = E[Y]$, and the slope vector $\beta_1^* = \Sigma^{-1} \sigma_{YX}^T$, where $[\sigma_{YX}]_{1 \times p} = E[(Y - \mu_Y)_{1 \times 1} (X - \mu_X)_{1 \times p}^T]$, with $\mu_Y = E[Y]$, and $\Sigma_{p \times p} = E \left[(X - \mu_X)_{p \times 1} (X - \mu_X)_{1 \times p}^T \right]$ denoting the matrix of variances and covariances of the regressor vector X . Hence, for every $x \in \mathbb{R}^p$, one can write

$$m_L(x) = \beta_0^* + (\beta_1^*)^T (x - \mu_X), \tag{2.6}$$

which can be equivalently expressed as

$$m_L(x) = E(Y) + \sigma_{YX} \Sigma^{-1} (x - \mu_X)$$

$$\begin{aligned}
&= \int_{\mathbb{R} \times \mathbb{R}^p} y[1 + (z - \mu_X)^T \Sigma^{-1}(x - \mu_X)] dF(z, y) \\
&= \int_{\mathbb{R} \times \mathbb{R}^p} y s(z, x) dF(z, y). \tag{2.7}
\end{aligned}$$

Since the weight function $s(z, x) = 1 + (z - \mu_X)^T \Sigma^{-1}(x - \mu_X)$ satisfies $\int_{\mathbb{R}^p \times \mathbb{R}} s(z, x) dF(z, y) = 1$, restricting our attention to the unit ball of the RKHS of X , one can consider the family of bivariate probability measures $\{P_x(dz, dy), x \in \mathbb{R}^p\}$, given by $P_x(dz, dy) = s(z, x) dF(z, y)$, $z \in \mathbb{R}^p$, $y \in \mathbb{R}$, for each $x \in \mathbb{R}^p$. Consider the marginal $P_x(dy) = \int_{\mathbb{R}^p} s(z, x) dF(z, y)$. Equation (2.7) can be symbolically rewritten as

$$\begin{aligned}
m_L(x) &= \int_{\mathbb{R}} y P_x(dy) = \arg \min_{\omega \in \mathbb{R}} \int_{\mathbb{R}} d_E^2(y, \omega) P_x(dy) \\
&= \arg \min_{\omega \in \mathbb{R}} \int_{\mathbb{R}} d_E^2(y, \omega) \int_{\mathbb{R}^p} s(z, x) dF(z, y) \\
&= \arg \min_{\omega \in \mathbb{R}} E \left[s(X, x) d_E^2(Y, \omega) \right]. \tag{2.8}
\end{aligned}$$

The weighted Fréchet mean approach proposed in Petersen and Müller (2019), under independent data, consists of replacing the Euclidean distance d_E by the distance d_Ω in an arbitrary metric space (Ω, d_Ω) , to cover the case where Y is evaluated in such a metric space (Ω, d_Ω) . That is,

$$m_L(x) = \arg \min_{\omega \in \Omega} E \left[s(X, x) d_\Omega^2(Y, \omega) \right] \tag{2.9}$$

[see Petersen and Müller (2019)]. Our proposal is formulated under dependent curve data, and corresponds to the case of $(\Omega, d_\Omega) = (\mathcal{C}_{\mathcal{M}}(\mathcal{T}), d_{\mathcal{C}_{\mathcal{M}}(\mathcal{T})})$, and $X \in (\mathcal{C}_{\mathcal{M}}(\mathcal{T}), d_{\mathcal{C}_{\mathcal{M}}(\mathcal{T})})$, extending the above Euclidean regressor framework to the \mathcal{M} -valued infinite-dimensional case.

3 Fréchet regression under dependent curve data in Riemannian manifolds

In Sect. 3.1, conditions (i)–(v) are formulated to provide a suitable geometrical and probabilistic scenario, allowing the definition of our weighted Fréchet mean based theoretical and empirical loss functions, and ensuring the existence and uniqueness of Fréchet curve means. Under these conditions, the curve regressor process is mapped into the time-varying tangent space. Fréchet weights are then computed in a regularized version of the RKHS of the log-mapped regressor process, obtained by applying a smoother matrix operator satisfying conditions (a)–(b) in Sect. 3.2. Finally, the theoretical and empirical loss functions are introduced in Sect. 3.3 under the conditions established in Sects. 3.1 and 3.2.

3.1 Model assumptions

The following conditions of geometrical nature will be considered:

- (i) \mathcal{M} is a d -dimensional compact and connected Riemannian submanifold of a Euclidean space \mathbb{R}^{d_0} , $d \leq d_0$, with geodesic distance $d_{\mathcal{M}}$ induced by the Euclidean metric.
- (ii) The sectional curvature of manifold \mathcal{M} is bounded, positive, and of smooth variation.

Remark 1 The exponential map is defined on the entire tangent space under (i) [see, e.g., Dai and Müller (2018)]. Under (ii), the geodesic distance between two points in the manifold is upper bounded by the Euclidean distance of their corresponding tangent vectors [see Assumption A2, and Proposition 1 in Dai and Müller (2018)].

Let $Y = \{Y_s, s \in \mathbb{Z}\}$ and $X = \{X_s, s \in \mathbb{Z}\}$ be the response Y and regressor X curve processes in the Riemannian manifold \mathcal{M} . Denote by $\mathcal{Y}_{\mathcal{C}_{\mathcal{M}}(\mathcal{T})} \subseteq (\mathcal{C}_{\mathcal{M}}(\mathcal{T}), d_{\mathcal{C}_{\mathcal{M}}(\mathcal{T})})$, and $\mathcal{X}_{\mathcal{C}_{\mathcal{M}}(\mathcal{T})} \subseteq (\mathcal{C}_{\mathcal{M}}(\mathcal{T}), d_{\mathcal{C}_{\mathcal{M}}(\mathcal{T})})$ the respective supports of their marginal probability measures (see conditions (iv)–(v) below). The following conditions are assumed on the bivariate curve process (X, Y) :

- (iii) For every time $s_i \in \mathbb{Z}$, the random Lipschitz constants $L_Y(Y_{s_i})$ and $L_X(X_{s_i})$ of Y_{s_i} and X_{s_i} are almost surely (a.s.) finite. The Lipschitz constants $L(\mu_{Y_{s_i}, \mathcal{M}})$ and $L(\mu_{X_{s_i}, \mathcal{M}})$ of the Fréchet means $\mu_{Y_{s_i}, \mathcal{M}}$ and $\mu_{X_{s_i}, \mathcal{M}}$ are also finite. Particularly, assume that $E \left[(L_X(X_{s_i}))^2 \right] < \infty$, and $E \left[(L_Y(Y_{s_i}))^2 \right] < \infty$, for any $s_i \in \mathbb{Z}$. Note that, for any curve $z(\cdot)$, $L(z) = \sup_{t \neq s} \frac{d_{\mathcal{M}}(z(t), z(s))}{|t-s|}$.
- (iv) The \mathcal{M} -valued bivariate curve process $\{(Y_s, X_s), s \in \mathbb{Z}\}$ is strictly stationary. Furthermore, $\{\log_{\mu_{X_0, \mathcal{M}}(t)}(X_s(t)), s \in \mathbb{Z}\}$ is mean-square ergodic in the first moment in the norm of \mathbb{H} , and in the second-order moments in the norm of the space $\mathcal{S}(\mathbb{H})$ of Hilbert–Schmidt operators on \mathbb{H} .
- (v) We assume that $X = \{X_s, s \in \mathbb{Z}\}$ and $Y = \{Y_s, s \in \mathbb{Z}\}$ have the same Fréchet functional mean. The supports of the marginal probability measures $dP_{X_0}(\cdot)$ and $dP_{Y_0}(\cdot)$ respectively induced by $X_0(\cdot)$ and Y_0 are included in the ball of the space $(\mathcal{C}_{\mathcal{M}}(\mathcal{T}), d_{\mathcal{C}_{\mathcal{M}}(\mathcal{T})})$, centered at the Fréchet functional mean $\mu_{X_0, \mathcal{M}} = \mu_{Y_0, \mathcal{M}}$ with radius $R = \inf_{t \in \mathcal{T}} \text{inj}_{\mu_{X_0, \mathcal{M}}(t)}$. Here, $\text{inj}_{\mu_{X_0, \mathcal{M}}(t)}$ denotes the injectivity radius of the exponential map whose origin is $\mu_{X_0, \mathcal{M}}(t)$, for each $t \in \mathcal{T}$.

The global regression methodology, based on the weighted Fréchet mean approach, arising from the linear correlation between the response and regressor in the Euclidean setting [see Sect. 2.1] has sense, since the log-mapped versions of both curve processes, X and Y , lie in the same time-varying tangent space, whose origin is the Fréchet functional mean $\mu_{X_0, \mathcal{M}} = \mu_{Y_0, \mathcal{M}}$ under conditions (iv)–(v).

Remark 2 Condition (v) ensures that, for every $t \in \mathcal{T}$, and $s_i \in \mathbb{Z}$, the geodesic connecting $X_{s_i}(t)$ and $\mu_{X_0, \mathcal{M}}(t)$ is unique, ensuring that the tangent vectors do not switch directions under small perturbations of $\mu_{X_0, \mathcal{M}}(t)$. The same assertion holds for $Y_{s_i}(t)$ and $\mu_{Y_0, \mathcal{M}}(t)$, $t \in \mathcal{T}$, $s_i \in \mathbb{Z}$. This condition is crucial in the implementation

of the weighted Fréchet mean approach from time correlated bivariate curve data evaluated in \mathcal{M} in a consistent way.

In practice, a curve clustering around the intrinsic Fréchet functional mean $\mu_{X_0, \mathcal{M}} = \mu_{Y_0, \mathcal{M}}$ is observed under conditions (i)–(v). The same feature holds around the empirical Fréchet functional mean $\widehat{\mu}_{X_0, \mathcal{M}}$ [see, e.g., Figs. 1, 2, 4 in the simulation study in Sect. 5]. See also Fig. 9 in Sect. 6, where the bivariate curve data (left-hand side), the empirical Fréchet curve means (center and right-hand side) are displayed. Note that this curve clustering is observed in most of the real-data problems cited in the Introduction. That is the case of flight trajectory data set (see, e.g., Sect. 5.2 of Dai and Müller (2018), where Riemannian functional principal component analysis (RFPCA) is applied).

3.2 Regularization of infinite-dimensional Fréchet weights

As commented, Fréchet weights are computed from the log-mapped regressor process $\left\{ \log_{\widehat{\mu}_{X_0, \mathcal{M}(\cdot)}}(X_s(\cdot)), s \in \mathbb{Z} \right\}$ in the time-varying tangent space. Denote by $\mu(t) = E \left[\log_{\mu_{X_0, \mathcal{M}(t)}}(X_0(t)) \right], t \in \mathcal{T}$, and by

$$\begin{aligned} \mathcal{R}_X &= E \left[\left(\log_{\mu_{X_0, \mathcal{M}(\cdot)}}(X_s(\cdot)) - \mu(\cdot) \right) \otimes \left(\log_{\mu_{X_0, \mathcal{M}(\cdot)}}(X_s(\cdot)) - \mu(\cdot) \right)^T \right] \\ &= E \left[\left(\log_{\mu_{X_0, \mathcal{M}(\cdot)}}(X_0(\cdot)) - \mu(\cdot) \right) \otimes \left(\log_{\mu_{X_0, \mathcal{M}(\cdot)}}(X_0(\cdot)) - \mu(\cdot) \right)^T \right], \end{aligned} \tag{3.10}$$

the matrix autocovariance operator of $\left\{ \log_{\mu_{X_0, \mathcal{M}(\cdot)}}(X_s(\cdot)), s \in \mathbb{Z} \right\}$. Its inverse, defining the semi-inner product $\langle f, g \rangle_{\widetilde{\mathbb{H}}} = \left\langle \mathcal{R}_X^{-1}(f), g \right\rangle_{\mathbb{H}}$, of the RKHS $\widetilde{\mathbb{H}} = \mathcal{R}_X^{1/2}(\mathbb{H})$ of $\left\{ \log_{\mu_{X_0, \mathcal{M}(\cdot)}}(X_s(\cdot)), s \in \mathbb{Z} \right\}$ is not bounded in the ambient Hilbert space \mathbb{H} . Fréchet weights are then computed in a regularized version $\mathcal{K}(\mathbb{H}) \subset \widetilde{\mathbb{H}}$ of \mathbb{H} (see condition (b) below), obtained from smoother matrix operator \mathcal{K} given by

$$\begin{aligned} \sqrt{\mathcal{K}}(\psi) &= \begin{bmatrix} \sqrt{\mathcal{K}} & 0 & \dots & 0 \\ 0 & \sqrt{\mathcal{K}} & \dots & 0 \\ \dots & \dots & \dots & \sqrt{\mathcal{K}} \end{bmatrix} \begin{bmatrix} \psi_1 \\ \vdots \\ \psi_{d_0} \end{bmatrix} \\ &= \left[\sqrt{\mathcal{K}}(\psi_1), \dots, \sqrt{\mathcal{K}}(\psi_{d_0}) \right]^T, \quad \forall \psi = (\psi_1, \dots, \psi_{d_0})^T \in \mathbb{H}. \end{aligned}$$

Thus, $\sqrt{\mathcal{K}}$ is a diagonal operator with constant functional entries equal to $\sqrt{\mathcal{K}}$, where \mathcal{K} is a trace self-adjoint integral operator on \mathbb{H} , satisfying

$$\mathcal{K}(\phi_n)(t) = \int_{\mathcal{T}} k(t, s)\phi_n(s)ds = \gamma_n\phi_n(t), \quad t \in \mathcal{T}, \quad \gamma_n > 0, \quad n \geq 1,$$

with $\sum_{n=1}^\infty \gamma_n = 1$. The norm induced by \mathcal{K} can be expressed in terms of the eigenvalue sequence $\{\gamma_n, n \in \mathbb{N}_0\}$ as

$$\|\psi\|_{\mathcal{K}}^2 = \langle \psi, \psi \rangle_{\mathcal{K}} = \sum_{i=1}^{d_0} \sum_{k \geq 1} \gamma_k |\phi_k(\psi_i)|^2 = \|\psi\|_{\tilde{H}_W}^2, \tag{3.11}$$

where we have denoted by \tilde{H}_W the separable Hilbert space of vector functions with finite $\|\cdot\|_{\mathcal{K}}$ -norm induced by the inner product $\langle \psi, \varphi \rangle_{\tilde{H}_W}$, given by, for $\psi = (\psi_1, \dots, \psi_{d_0})^T, \varphi = (\varphi_1, \dots, \varphi_{d_0})^T \in \mathbb{H} = H^{d_0}$,

$$\begin{aligned} \langle \psi, \varphi \rangle_{\tilde{H}_W} &= \left\langle \sqrt{\mathcal{K}}(\psi), \sqrt{\mathcal{K}}(\varphi) \right\rangle_{\mathbb{H}} = \int_T \left[\sqrt{\mathcal{K}}(\psi)(t) \right]^T \sqrt{\mathcal{K}}(\varphi)(t) dt \\ &= \sum_{i=1}^{d_0} \int_T \int_T k(t, s) \psi_i(t) \varphi_i(s) dt ds \\ &= \sum_{i=1}^{d_0} \sum_{k \geq 1} \gamma_k \phi_k(\psi_i) \phi_k(\varphi_i) = \sum_{i=1}^{d_0} \sum_{k \geq 1} \gamma_k \langle \phi_k, \psi_i \rangle_H \langle \phi_k, \varphi_i \rangle_H. \end{aligned} \tag{3.12}$$

Assume that $\{\gamma_n, n \geq 1\}$ satisfy

- (a) For every $f \in \mathbb{H}, \|f\|_{\mathbb{H}} \geq \|f\|_{\tilde{H}_W}$. Hence, $\mathbb{H} \subset \tilde{H}_W$ in a continuous way.
- (b) For every $\psi \in \sqrt{\mathcal{K}}(\mathbb{H}), \|\sqrt{\mathcal{K}}^{-1}(\psi)\|_{\mathbb{H}} \geq \|\psi\|_{\tilde{H}}$. Therefore, $(\sqrt{\mathcal{K}}(\mathbb{H}), \langle \cdot, \cdot \rangle_{\mathcal{K}^{-1}}) \subset (\tilde{H}, \langle \cdot, \cdot \rangle_{\tilde{H}})$ in a continuous way.

Hence, the following continuous inclusions (embeddings, denoted as \hookrightarrow) hold:

$$(\sqrt{\mathcal{K}}(\mathbb{H}), \langle \cdot, \cdot \rangle_{\mathcal{K}^{-1}}) \hookrightarrow (\tilde{H}, \langle \cdot, \cdot \rangle_{\tilde{H}}) \hookrightarrow (\mathbb{H}, \langle \cdot, \cdot \rangle_{\mathbb{H}}) \hookrightarrow (\tilde{H}_W, \langle \cdot, \cdot \rangle_{\tilde{H}_W}), \tag{3.13}$$

and the following regularized version of Fréchet weights is computed:

$$\begin{aligned} s(X_0(\cdot), x(\cdot)) &= \left[1 + \left\langle \log_{\mu_{X_0, \mathcal{M}(\cdot)}}(x(\cdot)) - \mu(\cdot), \sqrt{\mathcal{K}} \mathcal{R}_X^{-1} \left(\sqrt{\mathcal{K}} \left(\log_{\mu_{X_0, \mathcal{M}(\cdot)}}(X_0(\cdot)) - \mu(\cdot) \right) \right) \right\rangle_{\mathbb{H}} \right] \\ &= \left[1 + \left\langle \sqrt{\mathcal{K}} \left(\log_{\mu_{X_0, \mathcal{M}(\cdot)}}(x(\cdot)) - \mu(\cdot) \right), \sqrt{\mathcal{K}} \left(\log_{\mu_{X_0, \mathcal{M}(\cdot)}}(X_0(\cdot)) - \mu(\cdot) \right) \right\rangle_{\tilde{H}} \right]. \end{aligned} \tag{3.14}$$

Remark 3 Equation (3.14) restricts the support of the proposed theoretical Fréchet functional predictor $\hat{Y}(x(\cdot))$, in Eq. (3.16), and its empirical version $\hat{Y}_n(x(\cdot))$, in Eq. (3.21), to $\exp_{\mu_{X_0, \mathcal{M}(\cdot)}}(\sqrt{\mathcal{K}}(\mathbb{H})) \subset \exp_{\mu_{X_0, \mathcal{M}(\cdot)}}(\tilde{H}) \subset \mathcal{X}_{\mathcal{C}, \mathcal{M}(\mathcal{T})} \subset (\mathcal{C}_{\mathcal{M}(\mathcal{T})}, d_{\mathcal{C}, \mathcal{M}(\mathcal{T})})$, allowing their computation in a continuous way. This property is applied in the proof of Theorem 1 to derive uniform weak-consistency.

3.3 Formulation of the theoretical and empirical loss functions

Under conditions (i)–(v), let us consider, for every $z(\cdot) \in \mathcal{Y}_{\mathcal{C}_M(\mathcal{T})}$ and $x(\cdot) \in \mathcal{X}_{\mathcal{C}_M(\mathcal{T})}$, the loss function $M(z(\cdot), x(\cdot))$ given by:

$$M(z(\cdot), x(\cdot)) = E \left[s(X_0(\cdot), x(\cdot)) \int_{\mathcal{T}} [d_{\mathcal{M}}(Y_0(t), z(t))]^2 dt \right], \quad (3.15)$$

where the regularized Fréchet weights $s(X_0(\cdot), x(\cdot))$ have been introduced in Eq. (3.14). The proposed Fréchet predictor is obtained as the solution to the following minimization problem:

$$\hat{Y}(x(\cdot)) = \arg \min_{z(\cdot) \in \mathcal{Y}_{\mathcal{C}_M(\mathcal{T})}} M(z(\cdot), x(\cdot)), \quad x(\cdot) \in \mathcal{X}_{\mathcal{C}_M(\mathcal{T})}. \quad (3.16)$$

Let $((X_1(\cdot), Y_1(\cdot)), \dots, (X_n(\cdot), Y_n(\cdot)))$ be a bivariate functional sample of size n of correlated curves in time of the \mathcal{M} -valued response and regressor curve processes. For each $x(\cdot) \in \mathcal{X}_{\mathcal{C}_M(\mathcal{T})}$, and $z(\cdot) \in \mathcal{Y}_{\mathcal{C}_M(\mathcal{T})}$, the empirical version of (3.15), based on $((X_1(\cdot), Y_1(\cdot)), \dots, (X_n(\cdot), Y_n(\cdot)))$, is defined as

$$\begin{aligned} \hat{M}_n(z(\cdot), x(\cdot)) &= \frac{1}{n} \sum_{i=1}^n s_n(X_i(\cdot), x(\cdot)) \int_{\mathcal{T}} [d_{\mathcal{M}}(Y_i(t), z(t))]^2 dt, \\ &\forall z(\cdot) \in \mathcal{Y}_{\mathcal{C}_M(\mathcal{T})}, \quad x(\cdot) \in \mathcal{X}_{\mathcal{C}_M(\mathcal{T})}, \end{aligned} \quad (3.17)$$

where

$$\begin{aligned} s_n(X_i(\cdot), x(\cdot)) &= \left[1 + \left\langle \sqrt{\mathcal{K}} \left(\boldsymbol{y}_{x(\cdot), \bar{X}_n} \right), \hat{\mathcal{R}}_X^{-1} \left(\sqrt{\mathcal{K}} \left(\boldsymbol{y}_{X_i(\cdot), \bar{X}_n} \right) \right) \right\rangle_{\mathbb{H}} \right], \\ &\forall x(\cdot) \in \mathcal{X}_{\mathcal{C}_M(\mathcal{T})}, \quad i = 1, \dots, n, \end{aligned} \quad (3.18)$$

with

$$\begin{aligned} \hat{\mathcal{R}}_X &= \frac{1}{n} \sum_{i=1}^n \left[\log_{\hat{\mu}_{X_0, \mathcal{M}(\cdot)}}(X_i(\cdot)) - \bar{X}_n(\cdot) \right] \otimes \left[\log_{\hat{\mu}_{X_0, \mathcal{M}(\cdot)}}(X_i(\cdot)) - \bar{X}_n(\cdot) \right]^T \\ \boldsymbol{y}_{x(\cdot), \bar{X}_n} &= \log_{\hat{\mu}_{X_0, \mathcal{M}(\cdot)}}(x(\cdot)) - \bar{X}_n(\cdot), \quad x(\cdot) \in \mathcal{X}_{\mathcal{C}_M(\mathcal{T})}, \\ \boldsymbol{y}_{X_i(\cdot), \bar{X}_n} &= \log_{\hat{\mu}_{X_0, \mathcal{M}(\cdot)}}(X_i(\cdot)) - \bar{X}_n(\cdot), \quad i = 1, \dots, n, \\ \bar{X}_n(\cdot) &= \overline{\log_{\hat{\mu}_{X_0, \mathcal{M}(\cdot)}}(X(\cdot))} = \frac{1}{n} \sum_{i=1}^n \log_{\hat{\mu}_{X_0, \mathcal{M}(\cdot)}}(X_i(\cdot)) \\ \hat{\mu}_{X_0, \mathcal{M}(\cdot)} &= \arg \min_{\tilde{x}(\cdot) \in \mathcal{X}_{\mathcal{C}_M(\mathcal{T})}} \frac{1}{n} \sum_{i=1}^n \int_{\mathcal{T}} [d_{\mathcal{M}}(X_{S_i}(t), \tilde{x}(t))]^2 dt. \end{aligned} \quad (3.19)$$

$$(3.20)$$

Weak-consistency, in the supremum geodesic distance, of $\hat{\mu}_{X_0, \mathcal{M}(\cdot)}$ has been derived in Proposition 2 in Dai and Müller (2018) under curve independent data evaluated in

a manifold. Under conditions (i)–(v), this result holds under weak-dependent curve data evaluated in \mathcal{M} .

The empirical predictor is the solution of the following minimization problem:

$$\widehat{Y}_n(x(\cdot)) = \arg \min_{z(\cdot) \in \mathcal{Y}_{\mathcal{C}_{\mathcal{M}}(\mathcal{T})}} \widehat{M}_n(z(\cdot), x(\cdot)), \quad x(\cdot) \in \mathcal{X}_{\mathcal{C}_{\mathcal{M}}(\mathcal{T})}. \quad (3.21)$$

Conditions (i)–(v) ensure the existence and uniqueness of the theoretical \widehat{Y} , in (3.16), and empirical \widehat{Y}_n , in (3.21), Fréchet functional regression predictors (see, e.g., Theorem 2.1 in Afsari (2011)).

4 Weak-consistency of the predictor

The main result of this paper, Theorem 1 below, provides the uniform weak-consistency of the proposed empirical Fréchet functional predictor. To derive the proof of this result, the following additional conditions are assumed:

A.1 For each $x(\cdot) \in \mathcal{X}_{\mathcal{C}_{\mathcal{M}}(\mathcal{T})}$, and, for every $\varepsilon > 0$,

$$\inf_{\sup_{t \in \mathcal{T}} d_{\mathcal{M}}(z(t), \widehat{Y}(x(\cdot))(t)) > \varepsilon} M(z(\cdot), x(\cdot)) > M(\widehat{Y}(x(\cdot)), x(\cdot))$$

$$P \left(\inf_{\sup_{t \in \mathcal{T}} d_{\mathcal{M}}(z(t), \widehat{Y}_n(x(\cdot))(t)) > \varepsilon} \widehat{M}_n(z(\cdot), x(\cdot)) - \widehat{M}_n(\widehat{Y}_n(x(\cdot)), x(\cdot)) \geq \zeta(\varepsilon) \right) \rightarrow 1, \quad (4.22)$$

as $n \rightarrow \infty$, for certain $\zeta(\varepsilon) > 0$.

B.1 Assume that, for every $\varepsilon > 0$,

$$x(\cdot) \in \mathcal{X}_{\mathcal{C}_{\mathcal{M}}(\mathcal{T})}; \left\| \log_{\mu_{X_0, \mathcal{M}(\cdot)}}(x(\cdot)) \right\|_{\mathbb{H}} \leq B \quad \inf_{\sup_{t \in \mathcal{T}} d_{\mathcal{M}}(z(t), \widehat{Y}(x(\cdot))(t)) > \varepsilon} M(z(\cdot), x(\cdot)) - M(\widehat{Y}(x(\cdot)), x(\cdot)) > 0,$$

$$P \left(\inf_{x(\cdot) \in \mathcal{X}_{\mathcal{C}_{\mathcal{M}}(\mathcal{T})}; \left\| \log_{\widehat{\mu}_{X_0, \mathcal{M}(\cdot)}}(x(\cdot)) \right\|_{\mathbb{H}} \leq B \quad \inf_{\sup_{t \in \mathcal{T}} d_{\mathcal{M}}(z(t), \widehat{Y}_n(x(\cdot))(t)) > \varepsilon} \widehat{M}_n(z(\cdot), x(\cdot)) - \widehat{M}_n(\widehat{Y}_n(x(\cdot)), x(\cdot)) \geq \zeta(\varepsilon) \right) \rightarrow 1, \quad (4.23)$$

as $n \rightarrow \infty$, for certain $\zeta(\varepsilon) > 0$.

Remark 4 Under condition (v), the radius B in Eq. (4.23) can be the radius of the closed ball in the ambient Hilbert space \mathbb{H} containing the log-mapped support of the probability measure $dP_{X_0(\cdot)}$ induced by $X_0(\cdot)$.

C.1 The functional moments of the log-mapped bivariate curve process $\left\{ \left(\log_{\widehat{\mu}_{X_0, \mathcal{M}(\cdot)}}(X_s(\cdot)), \log_{\widehat{\mu}_{X_0, \mathcal{M}(\cdot)}}(Y_s(\cdot)) \right), s \in \mathbb{Z} \right\}$ satisfy the following

summability conditions:

$$\begin{aligned}
 & \sum_{u \in \mathbb{Z}} E \left[\left\| \log_{\mu_{X_0, \mathcal{M}(\cdot)}}(Y_0(\cdot)) - \log_{\mu_{X_0, \mathcal{M}(\cdot)}}(z(\cdot)) \right\|_{\mathbb{H}}^2 \right. \\
 & \quad \left. \times \left\| \log_{\mu_{X_0, \mathcal{M}(\cdot)}}(Y_u(\cdot)) - \log_{\mu_{X_0, \mathcal{M}(\cdot)}}(z(\cdot)) \right\|_{\mathbb{H}}^2 \right] < \infty. \\
 & \sum_{u \in \mathbb{Z}} E \left[\left\| \log_{\mu_{X_0, \mathcal{M}(\cdot)}}(Y_0(\cdot)) - \log_{\mu_{X_0, \mathcal{M}(\cdot)}}(z(\cdot)) \right\|_{\mathbb{H}}^2 \right. \\
 & \quad \times \left\| \log_{\mu_{X_0, \mathcal{M}(\cdot)}}(Y_u(\cdot)) - \log_{\mu_{X_0, \mathcal{M}(\cdot)}}(z(\cdot)) \right\|_{\mathbb{H}}^2 \\
 & \quad \times \left\| \log_{\mu_{X_0, \mathcal{M}(\cdot)}}(X_u(\cdot)) - \mu \right\|_{\mathbb{H}} \Big] < \infty, \\
 & \sum_{u \in \mathbb{Z}} E \left[\left\| \log_{\mu_{X_0, \mathcal{M}(\cdot)}}(Y_0(\cdot)) - \log_{\mu_{X_0, \mathcal{M}(\cdot)}}(z(\cdot)) \right\|_{\mathbb{H}}^2 \right. \\
 & \quad \times \left\| \log_{\mu_{X_0, \mathcal{M}(\cdot)}}(Y_u(\cdot)) - \log_{\mu_{X_0, \mathcal{M}(\cdot)}}(z(\cdot)) \right\|_{\mathbb{H}}^2 \\
 & \quad \times \left\| \log_{\mu_{X_0, \mathcal{M}(\cdot)}}(X_0(\cdot)) - \mu \right\|_{\mathbb{H}} \\
 & \quad \times \left\| \log_{\mu_{X_0, \mathcal{M}(\cdot)}}(X_u(\cdot)) - \mu \right\|_{\mathbb{H}} \Big] < \infty.
 \end{aligned}$$

Remark 5 In the proof of Theorem 1 below, condition C.1 allows proving pointwise mean-square consistency in the first argument of the empirical loss function, when the second-order moments of the log-mapped curve regressor process are totally specified. In the misspecified case, conditions (i)–(v) also allow proving consistency of the empirical loss function from this result, given the compactness of \mathcal{T} and \mathcal{M} . Condition A.1 is required to apply Corollary 3.2.3 in Van der Vaart and Wellner (1996) to obtain the weak-consistency of the empirical curve predictor in the supremum geodesic distance. Condition B.1 leads to the uniform weak-consistency of the empirical Fréchet functional predictor, applying uniform equicontinuity satisfied by the theoretical and empirical loss functions in the second argument under the assumed conditions in Sects. 3.1 and 3.2.

The following result provides the conditions ensuring the uniform weak-consistency, in the supremum geodesic distance, of the global empirical Fréchet curve predictor $\widehat{Y}_n(x(\cdot))$.

Theorem 1 *Under conditions (i)–(v) in Sect. 3.1, and conditions (a)–(b) in Sect. 3.2, if assumptions A.1 and C.1 hold, then,*

$$\sup_{t \in \mathcal{T}} d_{\mathcal{M}}(\widehat{Y}(x(\cdot))(t), \widehat{Y}_n(x(\cdot))(t)) = o_P(1), \tag{4.24}$$

for each $x(\cdot) \in \mathcal{X}_{\mathcal{C}, \mathcal{M}}(\mathcal{T})$.

Additionally, under assumption B.1,

$$\sup_{\|\log_{\mu_{X_0, \mathcal{M}(\cdot)}}(x(\cdot))\|_{\mathbb{H}} \leq B} \sup_{t \in \mathcal{T}} d_{\mathcal{M}}(\widehat{Y}(x(\cdot))(t), \widehat{Y}_n(x(\cdot))(t)) = o_P(1). \tag{4.25}$$

As commented in Remark 5, the proof of Theorem 1 (see Appendix A) follows from conditions A.1, B.1 and C.1, applying Corollary 3.2.3 in Van der Vaart and Wellner (1996), under the scenario defined by conditions (i)–(v) in Sect. 3.1, and conditions (a)–(b) in Sect. 3.2. Specifically, under condition C.1,

$$\widetilde{M}_n(z(\cdot), x(\cdot)) - M(z(\cdot), x(\cdot)) = o_P(1), \quad n \rightarrow \infty, \tag{4.26}$$

providing the pointwise weak-consistency in the first argument of the empirical loss function, when the second-order moments of the log-mapped curve regressor process are totally specified. Here,

$$\begin{aligned} \widetilde{M}_n(z(\cdot), x(\cdot)) &= \frac{1}{n} \sum_{i=1}^n \int_{\mathcal{T}} [d_{\mathcal{M}}(Y_i(t), z(t))]^2 dt \\ &\times \left[1 + \left\langle \sqrt{\mathcal{K}} \left(\log_{\mu_{X_0, \mathcal{M}(\cdot)}}(x(\cdot)) - \mu(\cdot) \right), \mathcal{R}_X^{-1} \left(\sqrt{\mathcal{K}} \left(\log_{\mu_{X_0, \mathcal{M}(\cdot)}}(X_i(\cdot)) - \mu(\cdot) \right) \right) \right\rangle_{\mathbb{H}} \right]. \end{aligned}$$

Conditions (i)–(v) lead to

$$\widehat{M}_n(z(\cdot), x(\cdot)) - \widetilde{M}_n(z(\cdot), x(\cdot)) = o_P(1), \quad n \rightarrow \infty. \tag{4.27}$$

Under conditions (i)–(v) and (a)–(b), keeping in mind the compactness of \mathcal{T} and \mathcal{M} , and Remark 4,

$$\sup_{d_{\mathcal{C}_{\mathcal{M}(\mathcal{T})}}(z_1(\cdot), z_2(\cdot)) \leq \delta} \left| \widehat{M}_n(z_1(\cdot), x(\cdot)) - \widehat{M}_n(z_2(\cdot), x(\cdot)) \right| = O_P(\delta). \tag{4.28}$$

From Eqs. (4.26)–(4.28), under condition A.1, Corollary 3.2.3 in Van der Vaart and Wellner (1996) leads to the weak-consistency of the Fréchet functional predictor in the supremum geodesic distance.

Condition B.1 allows to proving uniform weak-consistency, in the supremum geodesic distance, of the empirical Fréchet functional predictor applying Theorem 1.5.4 in Van der Vaart and Wellner (1996). Specifically, the proved equicontinuity of the theoretical loss function in the second argument, uniformly with respect to the first argument, leads to the uniform continuity of the theoretical predictor by applying first part of B.1. In addition, the equicontinuity in probability of the empirical loss function in the second argument, uniformly with respect to the first argument, leads to the uniform continuity in probability of the empirical predictor by applying the second part of B.2. Applying triangle inequality, Theorem 1.5.4 in Van der Vaart and Wellner (1996) leads to the desired result on uniform weak-consistency of the empirical Fréchet curve predictor.

Corollary 1 *If there exist positive constants $\mathcal{U}(Y)$ and $\mathcal{U}(X)$ such that*

$$\begin{aligned}
 P \left(\sup_{z(\cdot) \in \mathcal{Y}_{\mathcal{C}, \mathcal{M}}(\mathcal{T})} \left\| \log_{\mu_{X_0, \mathcal{M}(\cdot)}}(Y_0(\cdot)) - \log_{\mu_{X_0, \mathcal{M}(\cdot)}}(z(\cdot)) \right\|_{\mathbb{H}} \leq \mathcal{U}(Y) \right) &= 1, \\
 P \left(\left\| \log_{\mu_{X_0, \mathcal{M}(\cdot)}}(X_0(\cdot)) - \mu \right\|_{\mathbb{H}} \leq \mathcal{U}(X) \right) &= 1,
 \end{aligned}
 \tag{4.29}$$

which is the case under conditions (i)–(v), then, condition C.1 in Theorem 1 can be replaced by

$$\sum_{u \in \mathbb{Z}} E \left[\left\| \log_{\mu_{X_0, \mathcal{M}(\cdot)}}(Y_u(\cdot)) - \log_{\mu_{X_0, \mathcal{M}(\cdot)}}(z(\cdot)) \right\|_{\mathbb{H}}^2 \right] < \infty, \quad \forall z(\cdot) \in \mathcal{Y}_{\mathcal{C}, \mathcal{M}}(\mathcal{T}).
 \tag{4.30}$$

Remark 6 Note that, considering $\log_{\mu_{X_0, \mathcal{M}(\cdot)}}(z(\cdot)) = E \left[\log_{\mu_{X_0, \mathcal{M}(\cdot)}}(Y_0(\cdot)) \right]$ in Eq. (4.30), the log-mapped curve response process $\left\{ \log_{\mu_{X_0, \mathcal{M}(\cdot)}}(Y_s(\cdot)), s \in \mathbb{Z} \right\}$ displays Short Range Dependence (SRD) [see, e.g., Panaretos and Tavakoli (2013)]. Thus, Theorem 1 provides uniform weak-consistency of the empirical Fréchet curve predictor $\widehat{Y}_n(\cdot)$ in the supremum geodesic distance under weak-dependent curve data evaluated in \mathcal{M} .

5 Numerical examples

The finite functional sample size performance of $\widehat{Y}_n(x(\cdot))$, $x(\cdot) \in \mathcal{X}_{\mathcal{C}, \mathcal{M}}(\mathcal{T})$, is numerically illustrated in this section. We restrict our attention to the sphere \mathbb{S}_2 in \mathbb{R}^3 , and generate, at 1000 temporal nodes, a bivariate curve sample of size $n = 100$ of time correlated random spherical curves. We compute the pointwise quadratic geodesic distances between the original values of the response, and their Fréchet curve predictions. These values are summarized in terms of the empirical mean [see the left-hand side of Fig. 7], and the corresponding histogram [see the left-hand side of Fig. 8]. The empirical temporal means of the observed values of the quadratic geodesic curve errors at each sampled time are also computed [see the right-hand side of Fig. 7]. The corresponding histogram is displayed at the right-hand side of Fig. 8.

We have implemented, in MatLab language, a simulation algorithm based on vector diffusion process subordination by applying the inverse von Mises-Fisher distribution transform [see Algorithm 3 in the Supplementary Material of Jammalamadaka and Terdik (2022)]. We restrict our attention to the family of vector diffusion processes with linear drift obeying the following stochastic differential equation:

$$dX_t = \mu(t)X_t dt + \sigma(t, X_t)dW_t,
 \tag{5.31}$$

where X_t defines the vector process modeling the states of the system, $\mu(t)X_t$ represents the linear drift, and $\sigma(t, X_t) = D(t, X_t)V(t)$ defines the diffusion coefficient.

Thus, the coefficient $\sigma(t, X_t)$ is computed from a diagonal matrix D , where each element along the main diagonal is the corresponding element of the state vector X_t . The process W is vectorial Brownian motion with correlated components. This model has been generated with *sde*(\cdot) MatLab function (see Simulation of Multidimensional Market Models in Financial Toolbox of MatLab).

A sample of n strictly stationary and ergodic vector diffusion processes correlated in time is generated. This sample is mapped into the unit ball of the Banach space $\mathcal{C}_{\mathcal{X}}(\mathcal{T})$ of continuous vector functions with compact support contained in the interval \mathcal{T} taking values in the bounded set $\mathcal{X} \subset \mathbb{R}^3$. The inverse von Mises-Fisher transform is then pointwise applied to obtain a sample of the regressor curve process $X_{s_i}(t) = \left(X_{s_i}^{(1)}(t), X_{s_i}^{(2)}(t), X_{s_i}^{(3)}(t) \right)$, $t \in \mathcal{T}$, $i = 1, \dots, n$ (see Fig. 1). For each s_i , $i = 1, \dots, n$, and for every $t \in \mathcal{T}$, we compute the logarithm map of the generated sample values of the spherical curve regressor process as follows: For each $t \in \mathcal{T}$,

$$\begin{aligned} \log_{\widehat{\mu}_{X_0, \mathcal{M}}(t)}(X_{s_i}(t)) &= \frac{u(t, i)}{\|u(t, i)\|} d_{\mathbb{S}^d}(\widehat{\mu}_{X_0, \mathcal{M}}(t), X_{s_i}(t)), \\ u(t, i) &= X_{s_i}(t) - ([\widehat{\mu}_{X_0, \mathcal{M}}(t)]^T X_{s_i}(t)) \widehat{\mu}_{X_0, \mathcal{M}}(t), \end{aligned} \quad (5.32)$$

where $\widehat{\mu}_{X_0, \mathcal{M}}(\cdot)$ denotes, as before, the empirical Fréchet functional mean of X_0 . Finally, for $i = 1, \dots, n$, we generate the response curve process as

$$Y_{s_i}(t) = \exp_{\widehat{\mu}_{X_0, \mathcal{M}}(t)} \left(\Gamma \left(\log_{\widehat{\mu}_{X_0, \mathcal{M}}(\cdot)}(X_{s_i}(\cdot)) \right) (t) + \varepsilon_{s_i}(t) \right), \quad t \in \mathcal{T}, \quad (5.33)$$

where $\Gamma : \mathbb{H} \rightarrow \mathbb{H}$ is a bounded linear operator, with supremum norm less than one, and $\varepsilon = \{\varepsilon_i(\cdot), i \in \mathbb{Z}\}$ defines an \mathbb{H} -valued Gaussian strong-white noise, uncorrelated with the log-mapped regressors. Process ε has been generated in terms of the Karhunen–Loève expansion (see Dai and Müller (2018)).

Given the geometrical characteristics of the sphere, conditions (i)–(ii) hold. Condition (iii) is ensured by the sample path regularity properties displayed by the generated vector diffusion processes, and by the regularity properties of the eigenfunctions, involved in the Karhunen–Loève expansion of the strong Gaussian white noise process ε in the time-varying tangent space in (5.33). The assumed mean-square ergodicity in condition (iv) follows from the mixing conditions satisfied by the vector diffusion processes. The generation of the response process in the time-varying tangent space in (5.33) leads to its strict stationarity from the strict stationarity of the vector diffusion processes, and of ε in this example. Our choice of the concentration parameter involved in the implementation of the inverse von Mises–Fisher transform, and of the correlation structure of the generated vector-valued diffusion process ensures that condition (v) holds for the corresponding regressor process X . Condition (v) is also satisfied by the generated response curve process, given the dispersion of the curve values of ε in the time-varying tangent space is controlled by the truncated trace of its autocovariance operator, dominating the dispersion of the resulting exponential mapped curve values of the response process. Note that this trace is computed from the eigenvalues defining the variance of the random coefficients in the Karhunen–Loève

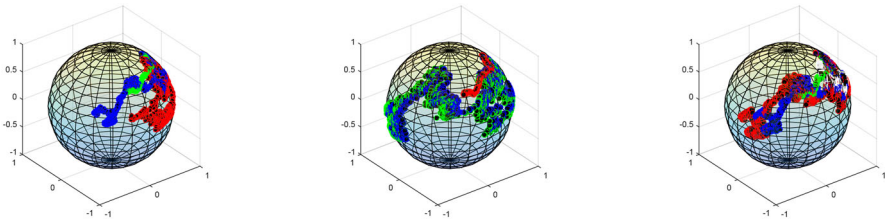


Fig. 1 Spherical curve values of the generated regressor process at times $s_i = 10, 20, 30, 40, 50, 60, 70, 80, 90, 100$. Three sampling times are represented on the left and center plots, and four on the right plot

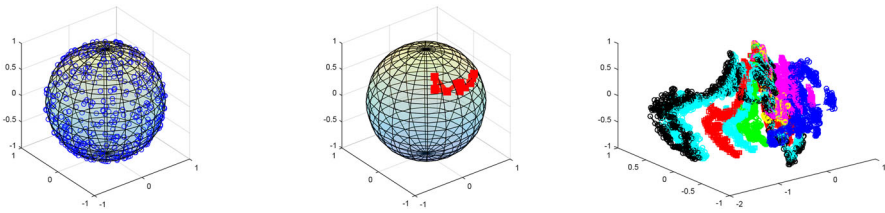


Fig. 2 Uniform spherical grid with 400 nodes (left-hand side), the empirical curve Fréchet mean $\mu_{\widehat{X}_0, \mathcal{M}}(\cdot)$ (center), and the response in the time-varying tangent space at times $s_i = 10, 20, 30, 40, 50, 60, 70, 80, 90, 100$ (right-hand side)

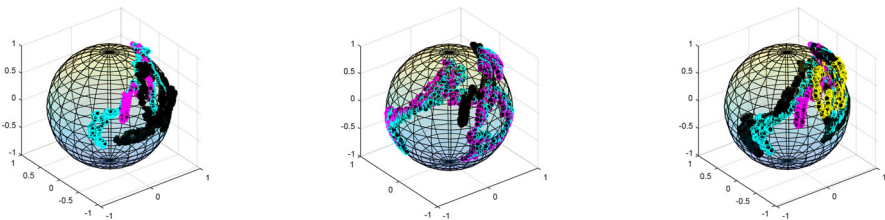


Fig. 3 Spherical curve values of the generated spherical curve response process at times $s_i = 10, 20, 30, 40, 50, 60, 70, 80, 90, 100$

expansion of ε . Furthermore, the selected eigenfunctions of the Dirichlet negative Laplace operator on a spatial interval are bounded and smooth.

The empirical Fréchet mean $\widehat{\mu}_{X_0, \mathcal{M}}(\cdot)$ in Eq. (3.20) is computed from a uniform spherical grid of 400 nodes (see Fig. 2). The time-varying Riemannian logarithm map with origin at $\widehat{\mu}_{X_0, \mathcal{M}}(\cdot)$ is applied to the generated spherical curve regressor values. As commented, these values are transformed via the dynamic functional linear model

$$\Gamma \left(\log_{\widehat{\mu}_{X_0, \mathcal{M}}(t)} \left(X_{s_i}(\cdot) \right) \right) (t) + \varepsilon_{s_i}(t), \quad t \in \mathcal{T}, \quad i = 1, \dots, n,$$

in the time-varying tangent space, leading to the log-mapped curve values of the response in those tangent spaces (see plot at the right-hand side of Fig. 2). The time-varying exponential map at the same origin $\widehat{\mu}_{X_0, \mathcal{M}}(\cdot)$ is then applied to them (see Figs. 3, and 4). The empirical Fréchet weights are also calculated as displayed in Fig. 5. Finally, the empirical weighted Fréchet mean function is obtained. The corresponding

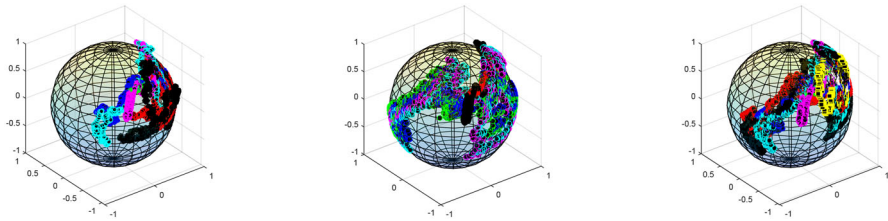


Fig. 4 Joint representation of spherical curve values of the generated spherical curve response and regressor processes at times $s_i = 10, 20, 30, 40, 50, 60, 70, 80, 90, 100$. Here, red, green, blue, and white colors are used for regressor spherical curve values, while black, magenta, cyan, and yellow colors are used for response spherical curve values

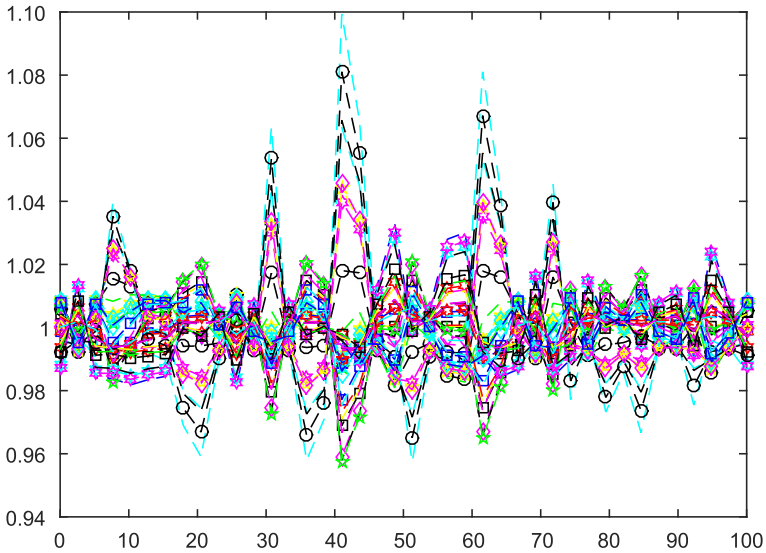


Fig. 5 The empirical Fréchet weights are plotted. The dashed lines displayed correspond to their evaluation from generated log-mapped sample curve regressor values at $s_i, i = 1, \dots, 100$, and for 40 log-mapped \mathcal{M} -curve arguments of the predictor

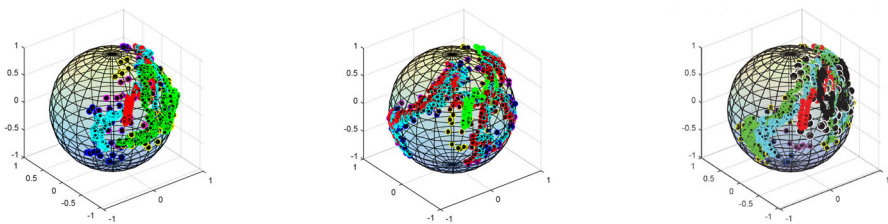


Fig. 6 The Fréchet predictor realizations, and the original responses are displayed at times $s_i = 10, 20, 30$ (left-hand side), $s_i = 40, 50, 60$ (center), and $s_i = 70, 80, 90, 100$ (right-hand side)

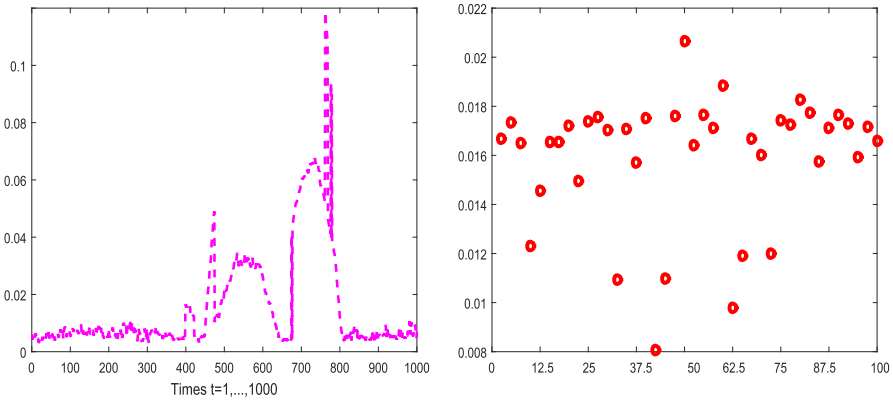


Fig. 7 The empirical mean of the quadratic geodesic curve errors (left-hand side), and the empirical temporal means of their pointwise values at each sampled time $s_i, i = 1, \dots, 100$ (right-hand side)

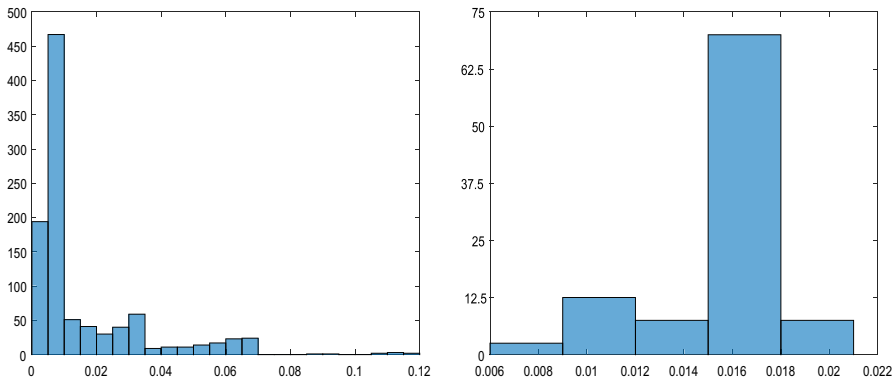


Fig. 8 Histogram of the quadratic geodesic curve error empirical mean values at the left-hand side. The histogram of the empirical temporal mean values is also plotted at the right-hand side

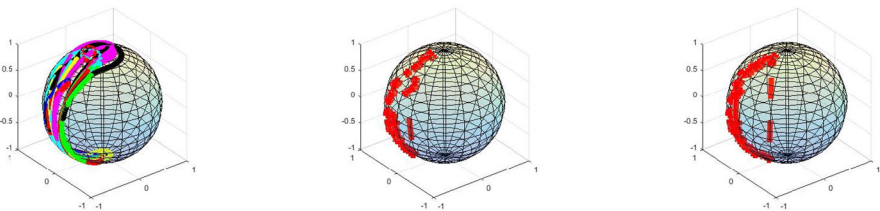


Fig. 9 Spherical bivariate curve data at times $t = 1, 11, 21, 31, 41, 51, 61, 71, 81$ (left-hand side). Empirical Fréchet curve mean of regressors (center) and of response (right-hand side)

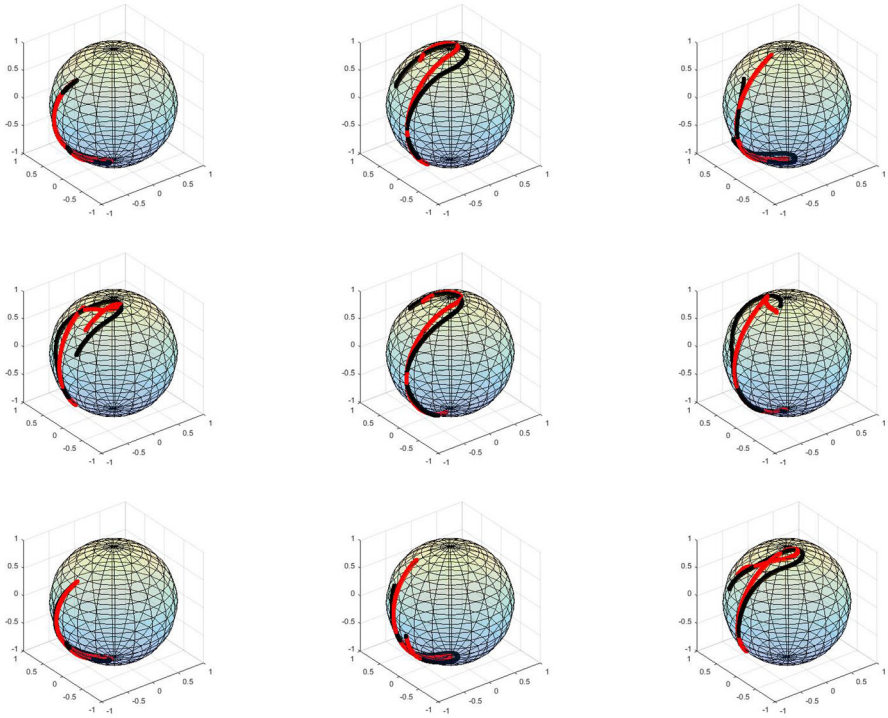


Fig. 10 Spherical bivariate curve data at times $t = 1, 12, 14, 25, 37, 49, 61, 73, 82$ (November, 1979). NASA's MAGSAT spacecraft (black curve), and magnetic field vector (red curve) spherical coordinates are displayed at 6000 temporal nodes for every sampled time

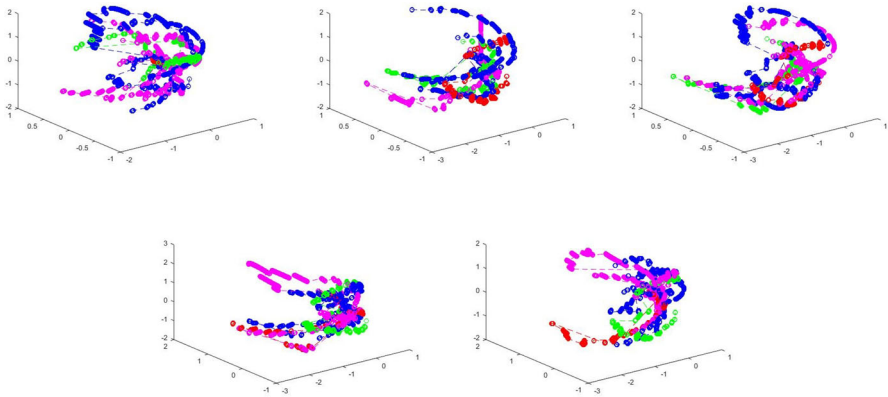


Fig. 11 Target log-mapped regressor curve observations at times $t = 1, 2, 4, 6, 8, 10$ for iteration one, at times $t = 1, 4, 7, 10, 18, 21$ for iteration 2, at times $t = 1, 4, 7, 10, 13, 16$ for iteration 3, at times $t = 1, 2, 3, 7, 10, 13$ for iteration 4, and at times $t = 3, 5, 7, 10, 15, 21$ for iteration 5

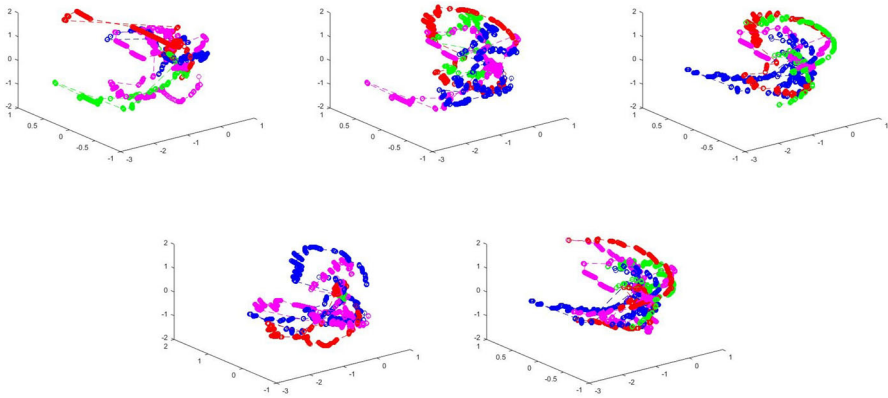


Fig. 12 Training log-mapped regressor curve observations at times $t = 1, 3, 6, 9, 12, 72$ for iteration one, at times $t = 1, 3, 6, 9, 12, 61$ for iteration 2, at times $t = 1, 3, 6, 9, 12, 66$ for iteration 3, at times $t = 10, 20, 30, 40, 50, 69$ for iteration 4, and at times $t = 10, 20, 30, 40, 50, 60$ for iteration 5

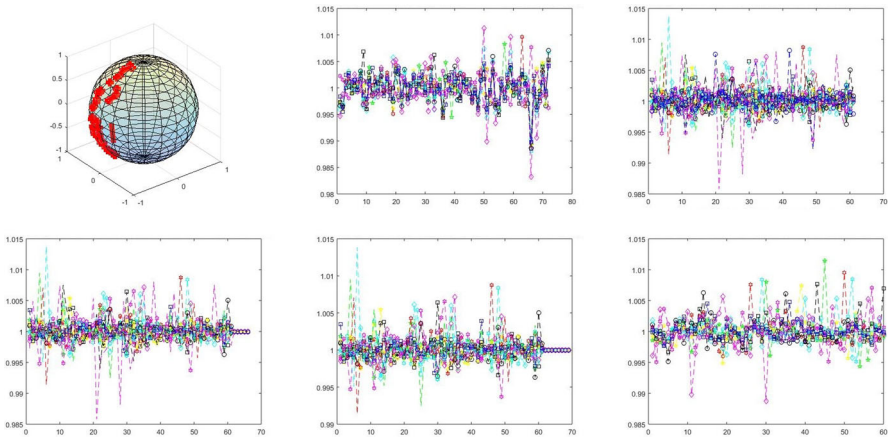


Fig. 13 Empirical Fréchet curve mean based on 82 spherical curve regressor observations, computed from a uniform spherical grid with 1000 nodes (top-left-hand-side). The remaining plots provide Fréchet weights at each one of the five iterations of the five fold cross validation algorithm implemented

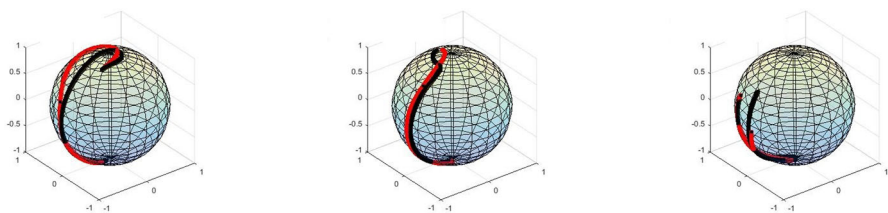


Fig. 14 Spherical Fréchet functional predictor (red curve) and response (black curve) at times $t_i, i = 1, 2, 3$ (corresponding to original observed times $t = 4, 11, 75$) of the target subsample at the first iteration of the five fold cross validation algorithm

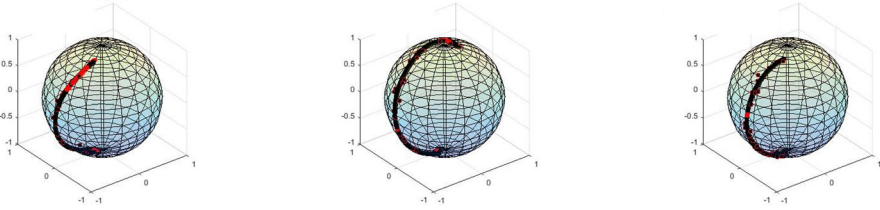


Fig. 15 Spherical Fréchet functional predictor (red curve) and response (black curve) at times t_i , $i = 1, 2, 3$ (corresponding to original observed times $t = 3, 6, 2$) of the target subsample at the second iteration of the five fold cross validation algorithm

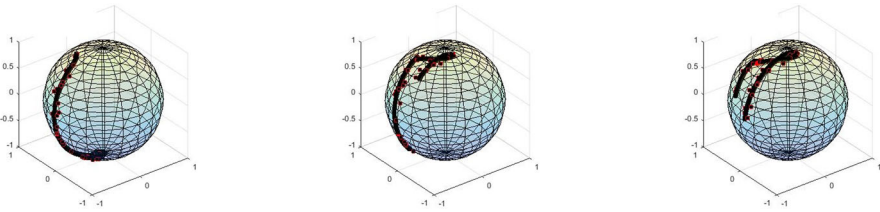


Fig. 16 Spherical Fréchet functional predictor (red curve) and response (black curve) at times t_i , $i = 1, 2, 3$ (corresponding to original observed times $t = 10, 25, 58$) of the target subsample at the third iteration of the five fold cross validation algorithm

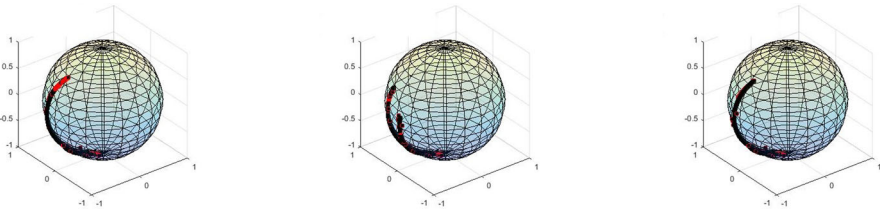


Fig. 17 Spherical Fréchet functional predictor (red curve) and response (black curve) at times t_i , $i = 1, 2, 3$ (corresponding to original observed times $t = 1, 28, 61$) of the target subsample at the fourth iteration of the five fold cross validation algorithm

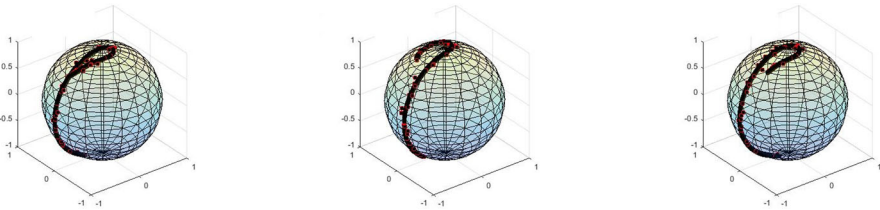


Fig. 18 Spherical Fréchet functional predictor (red curve) and response (black curve) at times t_i , $i = 1, 2, 3$ (corresponding to original observed times $t = 2, 12, 31$) of the target subsample at the fifth iteration of the five fold cross validation algorithm

Table 1 Temporal pointwise average of five fold cross validation functional error

TIMES	TPAF5fCVE	TIMES	TPAF5fCVE
T1	0.0037	T12	0.0027
T2	0.0036	T13	0.0030
T3	0.0034	T14	0.0023
T4	0.0037	T15	0.0022
T5	0.0031	T16	0.0021
T6	0.0039	T17	0.0013
T7	0.0039	T18	0.0016
T8	0.0036	T19	0.0015
T9	0.0040	T20	0.0016
T10	0.0036	T21	0.0014
T11	0.0030	T22	0.0006

Fréchet curve predictor is then computed as showed in Fig. 6. A good performance is observed when a functional sample of size $n = 100$ is considered, as displayed in Figs. 7 and 8, where Fréchet curve prediction errors are summarized.

6 Real-data example

It is well known that Earth's magnetic field protects Earth from solar wind that emanates from the sun. The three dimensional structure of this field is inferred from launched satellite measurements using three-axis magnetometers. World magnetic models are generated from these remote sensors combined over the last few decades. In particular, navigation and heading referencing systems can be improved from accurate information on geomagnetic field. Data from NASA's National Space Science Data Center are available in the period 02/11/1979–06/05/1980, recorded every half second, and correspond to the first satellite NASA's MAGSAT spacecraft, which orbited the earth every 88 min during seven months at around 400 km altitude. The available measurements during the days 3, 4, 5 of each month in the period 02/11/1979–06/05/1980 allow us to construct seven functional samples of size 82, 84, 83, 84, 85, 72 and 52, respectively. The elements of these samples are discretely observed at 6000 temporal nodes.

The five fold cross validation technique is implemented from these data sets to assess the performance of the proposed Fréchet functional regression prediction methodology. This section displays the results, based on a functional sample of size 82, reflecting the geocentric latitude and longitude of the spacecraft at 82 consecutive temporal intervals, containing 6000 equally spaced temporal nodes, during the days 3, 4, 5 of November, 1979, and reflecting the time-varying spherical coordinates of the magnetic field vector at the same temporal intervals and nodes. Both, the regressor and response spherical curve observations, share the azimuthal angle, and display different time-varying polar angles, as given at the top-right-hand-side plot in Fig. 4 of Sect. 9.1 in Di Marzio et al. (2014). Note that, in Di Marzio et al. (2014), a purely spatial

analysis is carried out ignoring time information. The five fold cross validation results for the remaining months are displayed in Appendix B.

As in the previous section, conditions (i)–(ii) are satisfied by $\mathcal{M} = \mathbb{S}_2 \subset \mathbb{R}^3$. Fig. 9 displays the spherical bivariate curve observations at times $t = 1, 11, 21, 31, 41, 51, 61, 71, 81$ at the left-hand side (see also Fig. 10, where some bivariate curve observations are displayed for different times). From these plots, conditions (iii)–(v) seem to be satisfied (see Remark 2). The empirical intrinsic Fréchet curve means, based on the regressors and the response curve observations, are respectively shown at the center, and at the right-hand side of Fig. 9. These plots also agree with the assumption of a common theoretical Fréchet curve mean for the marginal probability measure of the response and regressor process, as given in condition (v). The five fold cross validation technique is implemented from the log-mapped training and target spherical curve regressor subsamples in the time-varying tangent space (see Figs. 11 and 12), and from the corresponding training and target spherical curve response subsamples in \mathcal{M} . The displayed running of the five fold cross validation algorithm involves the training samples of sizes 72, 61, 66, 69, 60, and target samples of sizes 10, 21, 16, 13, 22, respectively.

Fréchet weights are computed from the training and target log-mapped regressor subsamples (see Fig. 13). Specifically, a discretized version of the empirical matrix covariance operator of the log-mapped curve regressors is computed from the training regressor subsample at each iteration of the five fold cross validation. Note that the row and column input vectors of the block matrix, approximating this empirical operator, are respectively evaluated in the training and target regressor subsamples. At each one of the 5 iterations of the five fold cross validation algorithm, the original spherical curve response values, and the corresponding spherical Fréchet functional predictions are plotted in Figs. 14, 15, 16, 17, and 18 at the first three target times. Finally, the average over the 6000 temporal nodes of the five fold cross validation functional error is displayed in Table 1, for the 22 Fréchet spherical curve predictions at target times $t = 2, 8, 12, 15, 22, 24, 26, 29, 31, 33, 40, 43, 45, 47, 53, 55, 56, 65, 67, 71, 76, 77$. This average is denoted as TPAF5fCVE in Table 1.

7 Final comments

This paper deals with global intrinsic Fréchet regression in the framework of $\mathcal{C}_{\mathcal{M}}(\mathcal{T})$ -valued bivariate curve processes, adopting the weighted Fréchet mean formulation introduced in Petersen and Müller (2019). Thus, we extend this formulation to the case of time correlated bivariate curve data evaluated in a compact Riemannian manifold. In particular, we extend the Euclidean regressor setting in Petersen and Müller (2019) to the \mathcal{M} -valued curve process framework, considering the metric space $(\mathcal{C}_{\mathcal{M}}(\mathcal{T}), d_{\mathcal{C}_{\mathcal{M}}(\mathcal{T})})$. Local linear Fréchet curve regression will be addressed in the manifold-valued bivariate curve process framework in a subsequent paper (see Petersen and Müller (2019), and Di Marzio et al. (2014) in the context of the local polynomial regression framework).

Appendices

The proof of the main result, Theorem 1, is provided in Appendix A. Appendix B shows the five fold cross validation results obtained since December, 1979, to May, 1980.

A Proof of Theorem 1

Proof For a fixed $x(\cdot) \in \mathcal{X}_{\mathcal{C}_{\mathcal{M}}(\mathcal{T})}$, under condition A.1, from Corollary 3.2.3 in Van der Vaart and Wellner (1996), it is sufficient to prove the convergence to zero in probability of

$$\sup_{z(\cdot) \in \mathcal{Y}_{\mathcal{C}_{\mathcal{M}}(\mathcal{T})}} \left| \widehat{M}_n(z(\cdot), x(\cdot)) - M(z(\cdot), x(\cdot)) \right|. \tag{1.34}$$

Indeed, from Theorem 1.5.4 in Van der Vaart and Wellner (1996), it is sufficient to prove

- (1) For each $x \in \mathcal{X}_{\mathcal{C}_{\mathcal{M}}(\mathcal{T})}$, and for every $z(\cdot) \in \mathcal{Y}_{\mathcal{C}_{\mathcal{M}}(\mathcal{T})}$,

$$\widehat{M}_n(z(\cdot), x(\cdot)) - M(z(\cdot), x(\cdot)) = o_P(1), \quad n \rightarrow \infty.$$

- (2) For each $x \in \mathcal{X}_{\mathcal{C}_{\mathcal{M}}(\mathcal{T})}$, and $z(\cdot) \in \mathcal{Y}_{\mathcal{C}_{\mathcal{M}}(\mathcal{T})}$, $\widehat{M}_n(z(\cdot), x(\cdot))$ is asymptotically equicontinuous in probability, i.e., for all $\varepsilon > 0$ and η , there exists a $\delta > 0$ which does not depend on $z(\cdot)$ such that

$$\limsup_n P \left(\sup_{d_{\mathcal{C}_{\mathcal{M}}(\mathcal{T})}(z(\cdot), y(\cdot)) \leq \delta} \left| \widehat{M}_n(z(\cdot), x(\cdot)) - \widehat{M}_n(y(\cdot), x(\cdot)) \right| > \varepsilon \right) < \eta. \tag{1.35}$$

To prove (1), we consider

$$\begin{aligned} \widetilde{M}_n(z(\cdot), x(\cdot)) &= \frac{1}{n} \sum_{i=1}^n \int_{\mathcal{T}} [d_{\mathcal{M}}(Y_i(t), z(t))]^2 dt \\ &\times \left[1 + \left\langle \sqrt{\mathcal{K}} \left(\log_{\mu_{x_0, \mathcal{M}(\cdot)}}(x(\cdot)) - \mu(\cdot) \right), \mathcal{R}_X^{-1} \left(\sqrt{\mathcal{K}} \left(\log_{\mu_{x_0, \mathcal{M}(\cdot)}}(X_i(\cdot)) - \mu(\cdot) \right) \right) \right\rangle_{\mathbb{H}} \right]. \end{aligned}$$

Under (iv), applying strictly stationarity, for each $x(\cdot) \in \mathcal{X}_{\mathcal{C}_{\mathcal{M}}(\mathcal{T})}$, and every $z(\cdot) \in \mathcal{Y}_{\mathcal{C}_{\mathcal{M}}(\mathcal{T})}$, $E \left[\widetilde{M}_n(z(\cdot), x(\cdot)) \right] = M(z(\cdot), x(\cdot))$. We also obtain

$$\begin{aligned} \text{Var}(\widetilde{M}_n(z(\cdot), x(\cdot))) &= \frac{1}{n} \sum_{u \in \{-(n-1), \dots, n-1\}} \left(1 - \frac{|u|}{n} \right) \\ &\times \left[\mathcal{R}_u^{(g(Y), g(Y))} + \mathcal{R}_u^{(g(Y), g(Y)h(X))} + \mathcal{R}_u^{(g(Y)h(X), g(Y))} + \mathcal{R}_u^{(g(Y)h(X), g(Y)h(X))} \right] \\ &\leq \frac{1}{n} \sum_{u \in \mathbb{Z}} \left[\mathcal{R}_u^{(g(Y), g(Y))} + \mathcal{R}_u^{(g(Y), g(Y)h(X))} + \mathcal{R}_u^{(g(Y)h(X), g(Y))} + \mathcal{R}_u^{(g(Y)h(X), g(Y)h(X))} \right] \tag{1.36} \end{aligned}$$

where

$$\begin{aligned}
 \mathcal{R}_u^{(g(Y),g(Y))} &= E \left[\left(\int_T [d_{\mathcal{M}}(Y_0(t), z(t))]^2 dt \right) \left(\int_T [d_{\mathcal{M}}(Y_u(t), z(t))]^2 dt \right) \right] \\
 \mathcal{R}_u^{(g(Y),g(Y)h(X))} &= E \left[\left(\int_T [d_{\mathcal{M}}(Y_0(t), z(t))]^2 dt \right) \left(\int_T [d_{\mathcal{M}}(Y_u(t), z(t))]^2 dt \right) \right. \\
 &\quad \times \left. \left\langle \sqrt{\mathcal{K}} \left(\log_{\mu_{X_0, \mathcal{M}(\cdot)}}(x(\cdot)) - \mu(\cdot) \right), \sqrt{\mathcal{K}} \left(\log_{\mu_{X_0, \mathcal{M}(\cdot)}}(X_u(\cdot)) - \mu(\cdot) \right) \right\rangle_{\tilde{H}} \right] \\
 \mathcal{R}_u^{(g(Y)h(X),g(Y))} &= E \left[\left(\int_T [d_{\mathcal{M}}(Y_0(t), z(t))]^2 dt \right) \left(\int_T [d_{\mathcal{M}}(Y_u(t), z(t))]^2 dt \right) \right. \\
 &\quad \times \left. \left\langle \sqrt{\mathcal{K}} \left(\log_{\mu_{X_0, \mathcal{M}(\cdot)}}(x(\cdot)) - \mu(\cdot) \right), \sqrt{\mathcal{K}} \left(\log_{\mu_{X_0, \mathcal{M}(\cdot)}}(X_0(\cdot)) - \mu(\cdot) \right) \right\rangle_{\tilde{H}} \right] \\
 \mathcal{R}_u^{(g(Y)h(X),g(Y)h(X))} &= E \left[\left(\int_T [d_{\mathcal{M}}(Y_0(t), z(t))]^2 dt \right) \left(\int_T [d_{\mathcal{M}}(Y_u(t), z(t))]^2 dt \right) \right. \\
 &\quad \times \left\langle \sqrt{\mathcal{K}} \left(\log_{\mu_{X_0, \mathcal{M}(\cdot)}}(x(\cdot)) - \mu(\cdot) \right), \sqrt{\mathcal{K}} \left(\log_{\mu_{X_0, \mathcal{M}(\cdot)}}(X_0(\cdot)) - \mu(\cdot) \right) \right\rangle_{\tilde{H}} \\
 &\quad \times \left. \left\langle \sqrt{\mathcal{K}} \left(\log_{\mu_{X_0, \mathcal{M}(\cdot)}}(x(\cdot)) - \mu(\cdot) \right), \sqrt{\mathcal{K}} \left(\log_{\mu_{X_0, \mathcal{M}(\cdot)}}(X_u(\cdot)) - \mu(\cdot) \right) \right\rangle_{\tilde{H}} \right]. \tag{1.37}
 \end{aligned}$$

Under (i)–(v), keeping in mind Remark 1, the following inequalities hold:

$$\begin{aligned}
 \mathcal{R}_u^{(g(Y),g(Y))} &\leq E \left[\left\| \log_{\mu_{X_0, \mathcal{M}(\cdot)}}(Y_0(\cdot)) - \log_{\mu_{X_0, \mathcal{M}(\cdot)}}(z(\cdot)) \right\|_{\mathbb{H}}^2 \right. \\
 &\quad \times \left. \left\| \log_{\mu_{X_0, \mathcal{M}(\cdot)}}(Y_u(\cdot)) - \log_{\mu_{X_0, \mathcal{M}(\cdot)}}(z(\cdot)) \right\|_{\mathbb{H}}^2 \right] \tag{1.38}
 \end{aligned}$$

$$\begin{aligned}
 \mathcal{R}_u^{(g(Y),g(Y)h(X))} &\leq \|\sqrt{\mathcal{K}}\mathcal{R}_X^{-1}\sqrt{\mathcal{K}}\|_{\mathcal{L}(\mathbb{H})} N(x(\cdot)) \\
 &\quad \times E \left[\left\| \log_{\mu_{X_0, \mathcal{M}(\cdot)}}(Y_0(\cdot)) - \log_{\mu_{X_0, \mathcal{M}(\cdot)}}(z(\cdot)) \right\|_{\mathbb{H}}^2 \right. \\
 &\quad \times \left\| \log_{\mu_{X_0, \mathcal{M}(\cdot)}}(Y_u(\cdot)) - \log_{\mu_{X_0, \mathcal{M}(\cdot)}}(z(\cdot)) \right\|_{\mathbb{H}}^2 \\
 &\quad \times \left. \left\| \log_{\mu_{X_0, \mathcal{M}(\cdot)}}(X_u(\cdot)) - \mu(\cdot) \right\|_{\mathbb{H}} \right] \tag{1.39}
 \end{aligned}$$

$$\begin{aligned}
 \mathcal{R}_u^{(g(Y)h(X),g(Y))} &\leq \|\sqrt{\mathcal{K}}\mathcal{R}_X^{-1}\sqrt{\mathcal{K}}\|_{\mathcal{L}(\mathbb{H})} N(x(\cdot)) \\
 &\quad \times E \left[\left\| \log_{\mu_{X_0, \mathcal{M}(\cdot)}}(Y_0(\cdot)) - \log_{\mu_{X_0, \mathcal{M}(\cdot)}}(z(\cdot)) \right\|_{\mathbb{H}}^2 \right. \\
 &\quad \times \left\| \log_{\mu_{X_0, \mathcal{M}(\cdot)}}(Y_u(\cdot)) - \log_{\mu_{X_0, \mathcal{M}(\cdot)}}(z(\cdot)) \right\|_{\mathbb{H}}^2 \\
 &\quad \times \left. \left\| \log_{\mu_{X_0, \mathcal{M}(\cdot)}}(X_0(\cdot)) - \mu(\cdot) \right\|_{\mathbb{H}} \right] \tag{1.40}
 \end{aligned}$$

$$\begin{aligned}
 \mathcal{R}_u^{(g(Y)h(X),g(Y)h(X))} &\leq \left[\|\sqrt{\mathcal{K}}\mathcal{R}_X^{-1}\sqrt{\mathcal{K}}\|_{\mathcal{L}(\mathbb{H})} N(x(\cdot)) \right]^2 \\
 &\quad \times E \left[\left\| \log_{\mu_{X_0, \mathcal{M}(\cdot)}}(Y_0(\cdot)) - \log_{\mu_{X_0, \mathcal{M}(\cdot)}}(z(\cdot)) \right\|_{\mathbb{H}}^2 \right. \\
 &\quad \times \left. \left\| \log_{\mu_{X_0, \mathcal{M}(\cdot)}}(Y_u(\cdot)) - \log_{\mu_{X_0, \mathcal{M}(\cdot)}}(z(\cdot)) \right\|_{\mathbb{H}}^2 \right]
 \end{aligned}$$

$$\begin{aligned} & \times \left\| \log_{\mathfrak{E}_{\mu_{X_0}, \mathcal{M}(\cdot)}} (X_0(\cdot)) - \mu(\cdot) \right\|_{\mathbb{H}} \\ & \times \left\| \log_{\mathfrak{E}_{\mu_{X_0}, \mathcal{M}(\cdot)}} (X_u(\cdot)) - \mu(\cdot) \right\|_{\mathbb{H}} \Big], \end{aligned} \tag{1.41}$$

where Cauchy–Schwarz inequality has been applied in the derivation of the upper bounds (1.39)–(1.41), keeping in mind condition (a)–(b) in Sect. 3.2, ensuring the bounded operator norm $\|\sqrt{\mathcal{K}}\mathcal{R}_{\bar{X}}^{-1}\sqrt{\mathcal{K}}\|_{\mathcal{L}(\mathbb{H})}$ on \mathbb{H} is finite. Here, $N(x(\cdot)) = \left\| \log_{\mathfrak{E}_{\mu_{X_0}, \mathcal{M}(\cdot)}} (x(\cdot)) - \mu(\cdot) \right\|_{\mathbb{H}}$. Under C.1, from (1.36), Eqs. (1.38)–(1.41) mean that

$$\tilde{M}_n(z(\cdot), x(\cdot)) - M(z(\cdot), x(\cdot)) = o_P(1), \quad n \rightarrow \infty.$$

Under conditions (i)–(v), conditions (A1) and (B1)–(B4) assumed in Proposition 2 in Dai and Müller (2018) hold. Weak-consistency in the supremum geodesic distance of the empirical Fréchet functional mean, under weak-dependent \mathcal{M} -valued curve data, can then be derived in a similar way to Proposition 2 in Dai and Müller (2018), applying the mean-square ergodicity of the log-mapped regressor process in condition (iv). Furthermore, under conditions (i)–(v),

$$\begin{aligned} & \widehat{M}_n(z(\cdot), x(\cdot)) - \tilde{M}_n(z(\cdot), x(\cdot)) \\ & = \frac{1}{n} \sum_{i=1}^n \left[\int_{\mathcal{T}} \left[d_{\mathcal{M}}^2(Y_i(t), z(t)) \right] dt \right] \left[\left\langle \sqrt{\mathcal{K}}(\mathbf{y}_{x(\cdot), \bar{X}_n(\cdot)}), \widehat{\mathcal{R}}_X^{-1}(\sqrt{\mathcal{K}}(\mathbf{y}_{X_i(\cdot), \bar{X}_n(\cdot)}) \right) \right\rangle_{\mathbb{H}} \right. \\ & \quad \left. - \left\langle \sqrt{\mathcal{K}}(\mathbf{y}_{x(\cdot), \mu(\cdot)}), \mathcal{R}_X^{-1}(\sqrt{\mathcal{K}}(\mathbf{y}_{X_i(\cdot), \mu(\cdot)}) \right) \right\rangle_{\mathbb{H}} \right] \\ & \leq [\text{diam}(\mathcal{M})]^2 |\mathcal{T}| \left[\left\langle \sqrt{\mathcal{K}}(\mathbf{y}_{x(\cdot), \bar{X}_n(\cdot)}), \widehat{\mathcal{R}}_X^{-1} \left(\sqrt{\mathcal{K}} \left(\frac{1}{n} \sum_{i=1}^n \mathbf{y}_{X_i(\cdot), \bar{X}_n(\cdot)} \right) \right) \right\rangle_{\mathbb{H}} \right. \\ & \quad \left. - \left\langle \sqrt{\mathcal{K}}(\mathbf{y}_{x(\cdot), \mu(\cdot)}), \mathcal{R}_X^{-1} \left(\sqrt{\mathcal{K}} \left(\frac{1}{n} \sum_{i=1}^n \mathbf{y}_{X_i(\cdot), \mu(\cdot)} \right) \right) \right\rangle_{\mathbb{H}} \right] = o_P(1), \end{aligned} \tag{1.42}$$

where $|\mathcal{T}| = \int_{\mathcal{T}} dt$, and

$$\begin{aligned} \mathbf{y}_{x(\cdot), \mu(\cdot)} & = \log_{\mathfrak{E}_{\mu_{X_0}, \mathcal{M}(\cdot)}} (x(\cdot)) - \mu(\cdot), \quad x(\cdot) \in \mathcal{X}_{\mathcal{C}_{\mathcal{M}}(\mathcal{T})}, \\ \mathbf{y}_{X_i(\cdot), \mu(\cdot)} & = \log_{\mathfrak{E}_{\mu_{X_0}, \mathcal{M}(\cdot)}} (X_i(\cdot)) - \mu(\cdot), \quad i = 1, \dots, n, \end{aligned} \tag{1.43}$$

with $\mathbf{y}_{x(\cdot), \bar{X}_n(\cdot)}$ and $\mathbf{y}_{X_i(\cdot), \bar{X}_n(\cdot)}$ being introduced in Eq. (3.19).

Now to prove (2), under conditions (iv)–(v) in Sect. 3.1 and (a)–(b) in Sect. 3.2, applying, in particular, men-square ergodicity of the log-mapped regressor process X in condition (iv), for n sufficiently large, and for $z_1(\cdot), z_2(\cdot) \in \mathcal{Y}_{\mathcal{C}_{\mathcal{M}}(\mathcal{T})}$,

$$\begin{aligned} & \left| \widehat{M}_n(z_1(\cdot), x(\cdot)) - \widehat{M}_n(z_2(\cdot), x(\cdot)) \right| \\ & \leq \frac{1}{n} \sum_{i=1}^n \left| \left\langle \sqrt{\mathcal{K}}(\mathbf{y}_{x(\cdot), \bar{X}_n(\cdot)}), \widehat{\mathcal{R}}_X^{-1}(\sqrt{\mathcal{K}}(\mathbf{y}_{X_i(\cdot), \bar{X}_n(\cdot)}) \right) \right\rangle_{\mathbb{H}} \right| \\ & \quad \times \left| \int_{\mathcal{T}} \left[d_{\mathcal{M}}^2(Y_i(t), z_1(t)) - d_{\mathcal{M}}^2(Y_i(t), z_2(t)) \right] dt \right| \end{aligned}$$

$$\begin{aligned}
 &= \frac{1}{n} \sum_{i=1}^n \left| \left\langle \sqrt{\mathcal{K}} \left(\boldsymbol{y}_{x(\cdot), \bar{X}_n(\cdot)} \right), \widehat{\mathcal{R}}_X^{-1} \left(\sqrt{\mathcal{K}} \left(\boldsymbol{y}_{X_i(\cdot), \bar{X}_n(\cdot)} \right) \right) \right\rangle_{\mathbb{H}} \right| \\
 &\times \left| \int_{\mathcal{T}} [d_{\mathcal{M}}(Y_i(t), z_1(t)) - d_{\mathcal{M}}(Y_i(t), z_2(t))] \right. \\
 &\times [d_{\mathcal{M}}(Y_i(t), z_1(t)) + d_{\mathcal{M}}(Y_i(t), z_2(t))] dt \\
 &\leq 2 \text{diam}(\mathcal{M}) \sup_{t \in \mathcal{T}} d_{\mathcal{M}}(z_1(t), z_2(t)) |\mathcal{T}| \\
 &\times \frac{1}{n} \sum_{i=1}^n \left| \left\langle \sqrt{\mathcal{K}} \left(\boldsymbol{y}_{x(\cdot), \bar{X}_n(\cdot)} \right), \widehat{\mathcal{R}}_X^{-1} \left(\sqrt{\mathcal{K}} \left(\boldsymbol{y}_{X_i(\cdot), \bar{X}_n(\cdot)} \right) \right) \right\rangle_{\mathbb{H}} \right| \\
 &\leq 2 \text{diam}(\mathcal{M}) \sup_{t \in \mathcal{T}} d_{\mathcal{M}}(z_1(t), z_2(t)) |\mathcal{T}| \\
 &\times \sup_{i \in \mathbb{Z}} \left\| \boldsymbol{y}_{X_i(\cdot), \bar{X}_n(\cdot)} \right\|_{\mathbb{H}} \left\| \sqrt{\mathcal{K}} \widehat{\mathcal{R}}_X^{-1} \sqrt{\mathcal{K}} \right\|_{\mathcal{L}(\mathbb{H})} \left\| \boldsymbol{y}_{x(\cdot), \bar{X}_n(\cdot)} \right\|_{\mathbb{H}} \\
 &= \mathcal{O}_P \left(\sup_{t \in \mathcal{T}} d_{\mathcal{M}}(z_1(t), z_2(t)) \right). \tag{1.44}
 \end{aligned}$$

Note that, under condition (v), $\sup_{i \in \mathbb{Z}} \left\| \boldsymbol{y}_{X_i(\cdot), \bar{X}_n(\cdot)} \right\|_{\mathbb{H}} < \infty$ (see Remark 4). Hence,

$$\sup_{d_{\mathcal{C}_{\mathcal{M}}(\mathcal{T})}(z_1(\cdot), z_2(\cdot)) \leq \delta} \left| \widehat{M}_n(z_1(\cdot), x(\cdot)) - \widehat{M}_n(z_2(\cdot), x(\cdot)) \right| = \mathcal{O}_P(\delta). \tag{1.45}$$

From Corollary 3.2.3 in Van der Vaart and Wellner (1996), under assumption A.1 Eq. (4.24) holds. In particular, the generalized process

$$\left\{ Z_n(x(\cdot)) = \sup_{t \in \mathcal{T}} d_{\mathcal{M}} \left(\widehat{Y}(x(\cdot))(t), \widehat{Y}_n(x(\cdot))(t) \right), x(\cdot) \in \mathcal{X}_{\mathcal{C}_{\mathcal{M}}(\mathcal{T})} \right\}$$

satisfies $Z_n(x(\cdot)) = o_P(1)$, for each $x(\cdot) \in \mathcal{X}_{\mathcal{C}_{\mathcal{M}}(\mathcal{T})}$.

To prove (4.25) under assumption B.1, since we are evaluating our predictors on the exponential map $\exp_{\mu_{X_0, \mathcal{M}(\cdot)}}(\mathcal{B}_{\mathbb{H}}(0, B))$ of the ball $\mathcal{B}_{\mathbb{H}}(0, B)$ with center 0 and radius $B > 0$ in \mathbb{H} (see also Remark 4), from Theorem 1.5.4 in Van der Vaart and Wellner (1996), it is sufficient to prove that, for any $S > 0$ and as $\delta \rightarrow 0$,

$$\limsup_{n \rightarrow \infty} P \left(\sup_{\left\| \log_{\mu_{X_0, \mathcal{M}(\cdot)}}(x(\cdot)) - \log_{\mu_{X_0, \mathcal{M}(\cdot)}}(y(\cdot)) \right\|_{\mathbb{H}} \leq \delta} |Z_n(x(\cdot)) - Z_n(y(\cdot))| > 2S \right) \rightarrow 0. \tag{1.46}$$

Hence, since from triangle inequality,

$$|Z_n(x(\cdot)) - Z_n(y(\cdot))| \leq \sup_{t \in \mathcal{T}} d_{\mathcal{M}} \left(\widehat{Y}(x(\cdot))(t), \widehat{Y}(y(\cdot))(t) \right)$$

$$+ \sup_{t \in \mathcal{T}} d_{\mathcal{M}}(\widehat{Y}_n(x(\cdot))(t), \widehat{Y}_n(y(\cdot))(t)), \text{ a.s.} \quad (1.47)$$

it is sufficient to prove that $\widehat{Y}(x(\cdot))$ is uniformly continuous over $\exp_{\mu_{X_0, \mathcal{M}(\cdot)}}(\mathcal{B}_{\mathbb{H}}(0, B))$, and that

$$\limsup_{n \rightarrow \infty} P \left(\sup_{y(\cdot) \in \widetilde{\mathcal{B}}_{x(\cdot)}(\delta'), x(\cdot) \in \exp_{\mu_{X_0, \mathcal{M}(\cdot)}}(\mathcal{B}_{\mathbb{H}}(0, B))} \sup_{t \in \mathcal{T}} d_{\mathcal{M}}(\widehat{Y}_n(x(\cdot))(t), \widehat{Y}_n(y(\cdot))(t)) > S \right) \rightarrow 0, \quad (1.48)$$

keeping in mind that under conditions (ii) and (v) in Sect. 3.1, given a $\delta > 0$, there exists $\delta' \leq \delta$, such that

$$\begin{aligned} \exp_{\mu_{X_0, \mathcal{M}(\cdot)}}(\mathcal{B}_{\mathbb{H}}(\log_{\mu_{X_0, \mathcal{M}(\cdot)}}(x(\cdot)), \delta)) &= \widetilde{\mathcal{B}}_{\mathcal{C}_{\mathcal{M}}(\mathcal{T}), d_{\mathcal{C}_{\mathcal{M}}(\mathcal{T})}}(x(\cdot), \delta') = \widetilde{\mathcal{B}}_{x(\cdot)}(\delta') \\ &:= \left\{ y(\cdot) \in \mathcal{X}_{\mathcal{C}_{\mathcal{M}}(\mathcal{T})}; \left\| \log_{\mu_{X_0, \mathcal{M}(\cdot)}}(x(\cdot)) - \log_{\mu_{X_0, \mathcal{M}(\cdot)}}(y(\cdot)) \right\|_{\mathbb{H}} \leq \delta \right\}. \end{aligned} \quad (1.49)$$

Let $\delta > 0$, and consider $x(\cdot) \in \exp_{\mu_{X_0, \mathcal{M}(\cdot)}}(\mathcal{B}_{\mathbb{H}}(0, B))$, and $y(\cdot) \in \widetilde{\mathcal{B}}_{x(\cdot)}(\delta')$ (see Eq. (1.49)). Under conditions (i)-(v), and (a) and (b) (see also Eq. (3.13) in Sect. 3.2), by the form of the loss function M , applying continuity of operator $\sqrt{\mathcal{K}}\mathcal{R}_X^{-1}\sqrt{\mathcal{K}}$, as $\delta \rightarrow 0$,

$$\begin{aligned} &\sup_{z(\cdot) \in \mathcal{Y}_{\mathcal{C}_{\mathcal{M}}(\mathcal{T})}} |M(z(\cdot), x(\cdot)) - M(z(\cdot), y(\cdot))| \\ &\leq \sup_{z(\cdot) \in \mathcal{Y}_{\mathcal{C}_{\mathcal{M}}(\mathcal{T})}} E \left[\left(\int_{\mathcal{T}} d_{\mathcal{M}}^2(Y_0(t), z(t)) dt \right) \|\boldsymbol{\gamma}_{X_0(\cdot), \mu(\cdot)}\|_{\mathbb{H}} \right] \left\| \sqrt{\mathcal{K}}\mathcal{R}_X^{-1}\sqrt{\mathcal{K}} \right\|_{\mathcal{L}(\mathbb{H})} \\ &\quad \times \|\boldsymbol{\gamma}_{x(\cdot), \mu(\cdot)} - \boldsymbol{\gamma}_{y(\cdot), \mu(\cdot)}\|_{\mathbb{H}} \leq [\text{diam}(\mathcal{M})]^2 |\mathcal{T}| E \left[\|\boldsymbol{\gamma}_{X_0(\cdot), \mu(\cdot)}\|_{\mathbb{H}} \right] \\ &\quad \times \left\| \sqrt{\mathcal{K}}\mathcal{R}_X^{-1}\sqrt{\mathcal{K}} \right\|_{\mathcal{L}(\mathbb{H})} \|\boldsymbol{\gamma}_{x(\cdot), \mu(\cdot)} - \boldsymbol{\gamma}_{y(\cdot), \mu(\cdot)}\|_{\mathbb{H}} \rightarrow 0, \end{aligned} \quad (1.50)$$

where $\boldsymbol{\gamma}_{X_0(\cdot), \mu(\cdot)}$ and $\boldsymbol{\gamma}_{x(\cdot), \mu(\cdot)}$ have been introduced in Eq. (1.43). The first part of Assumption B.1 then implies that \widehat{Y} is continuous over the ball $\exp_{\mu_{X_0, \mathcal{M}(\cdot)}}(\mathcal{B}_{\mathbb{H}}(0, B))$ in the supremum geodesic distance, hence, uniformly continuous.

To prove (1.48), applying conditions (iv)–(v) (see also Remark 4), we first have to note that if $d_{\mathcal{C}, \mathcal{M}(\mathcal{T})}(\widehat{Y}_n(x(\cdot)), \widehat{Y}_n(y(\cdot))) > \varepsilon$, under B.1, the following inequality holds in probability

$$\zeta \leq \sup_{\|\log_{\mu_{X_0, \mathcal{M}(\cdot)}}(x(\cdot)) - \log_{\mu_{X_0, \mathcal{M}(\cdot)}}(y(\cdot))\| < \delta} \sup_{z(\cdot) \in \mathcal{Y}_{\mathcal{C}, \mathcal{M}(\mathcal{T})}} |\widehat{M}_n(z(\cdot), x(\cdot)) - \widehat{M}_n(z(\cdot), y(\cdot))|, \tag{1.51}$$

for certain $\zeta > 0$. Furthermore, from the expression of \widehat{M}_n in Eq. (3.17), for $x(\cdot), y(\cdot)$, such that $\|\log_{\mu_{X_0, \mathcal{M}(\cdot)}}(x(\cdot)) - \log_{\mu_{X_0, \mathcal{M}(\cdot)}}(y(\cdot))\| < \delta$, for n sufficiently large,

$$\begin{aligned} & \sup_{z(\cdot) \in \mathcal{Y}_{\mathcal{C}, \mathcal{M}(\mathcal{T})}} |\widehat{M}_n(z(\cdot), x(\cdot)) - \widehat{M}_n(z(\cdot), y(\cdot))| \leq [\text{diam}(\mathcal{M})]^2 |\mathcal{T}| \sup_{i \in \mathbb{Z}} \|\boldsymbol{\gamma}_{X_i(\cdot), \bar{X}_n(\cdot)}\|_{\mathbb{H}} \\ & \times \left\| \sqrt{\widehat{\mathcal{K}}_X} \widehat{\mathcal{R}}_X^{-1} \sqrt{\widehat{\mathcal{K}}} \right\|_{\mathcal{L}(\mathbb{H})} \left\| \boldsymbol{\gamma}_{x(\cdot), \bar{X}_n(\cdot)} - \boldsymbol{\gamma}_{y(\cdot), \bar{X}_n(\cdot)} \right\|_{\mathbb{H}} = \mathcal{O}_P(\delta). \end{aligned} \tag{1.52}$$

Equation (1.48) then follows from Eqs. (1.51) and (1.52), when $\delta \rightarrow 0$, keeping in mind Eq. (1.49), and the second part of condition B.1 (see again Corollary 3.2.3 in Van der Vaart and Wellner (1996)).

□

B Analysis of the remaining months December, 1979–May, 1980

Similar cross validation results are obtained for each month in the period December, 1979–May, 1980, considering the data set available at NASA’s National Space Science Data Center. Missing data affect the analysis of these months. As commented, the sample size for each month is different, with May being the most affected month by missing data, although it has not prevented its inclusion in our analysis. We have adopted the criterion that all curves should have 6000 consecutive time nodes. For each month, the starting time of the curves was taken randomly from the excess nodes of the corresponding multiple of 6000 nodes contained in days 3–5 of the month considered. This, together with the existence of missing data, means that, a priori, monthly translations of curve samples likely do not correspond to identical time intervals. Figures 19–20 display spherical bivariate curve data during these remaining months. Empirical intrinsic Fréchet functional means of regressors are shown in Fig. 21, and five fold cross validation quadratic angular functional errors are provided in Fig. 22.

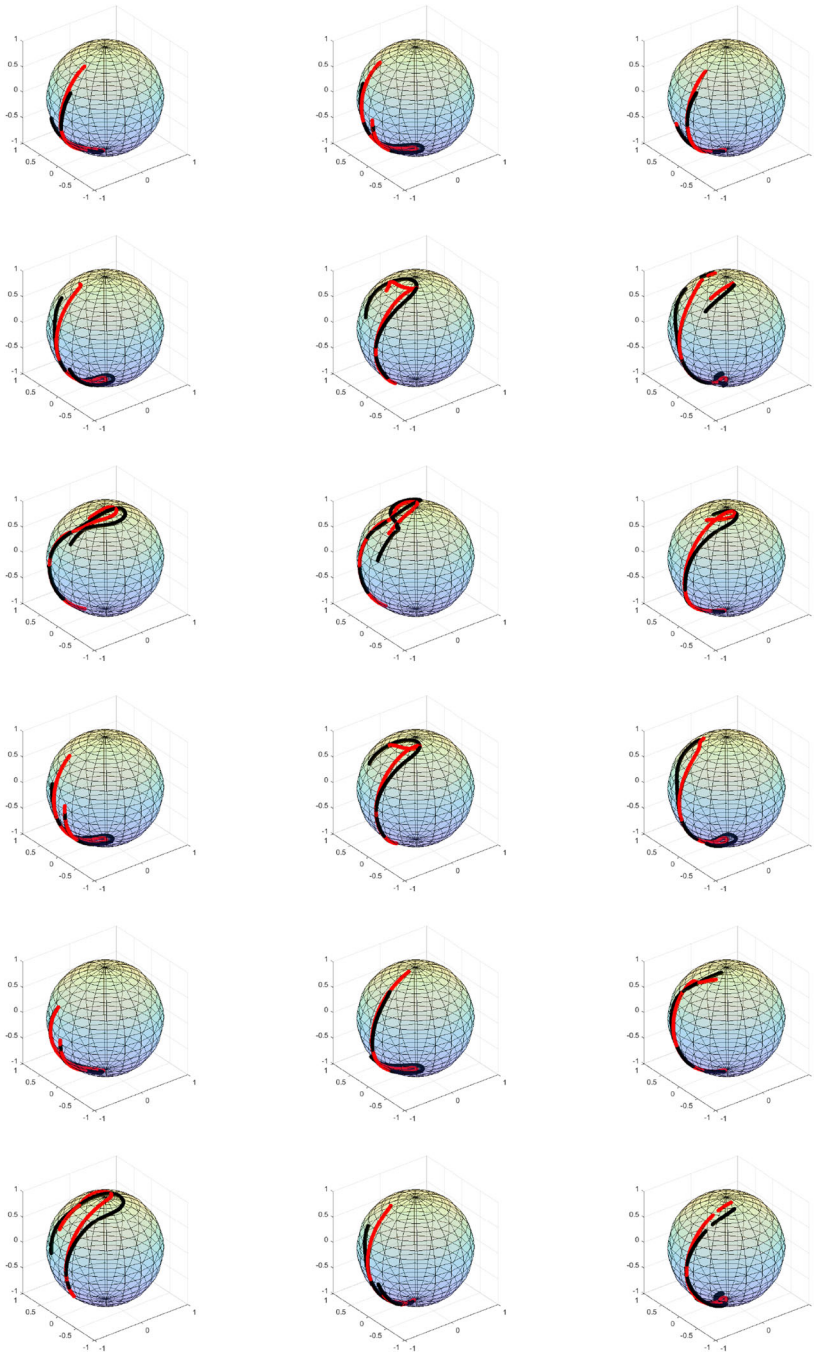


Fig. 19 Spherical bivariate curve data at times $t = 1, 15, 29, 43, 57, 71$ for December (first two lines), January (second two lines), and February (last two lines), representing NASA's MAGSAT spacecraft (black curve), and magnetic field vector (red curve). The spherical coordinates are displayed at 6000 temporal nodes for every sampled time

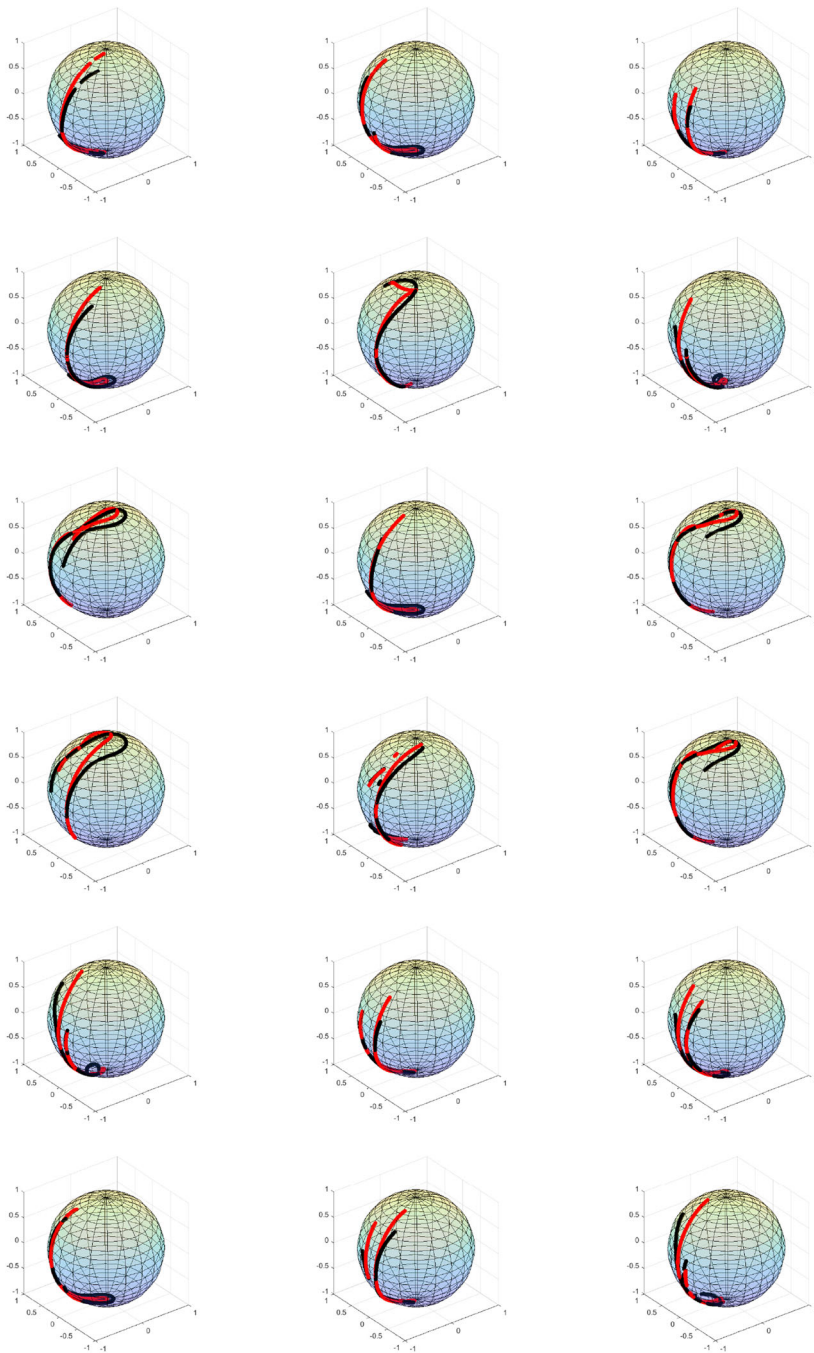


Fig. 20 Spherical bivariate curve data at times $t = 1, 15, 29, 43, 57, 71$ for March (first two lines) and April (second two lines), and at times $t = 1, 15, 29, 43, 48, 52$ for May (last two lines), representing NASA's MAGSAT spacecraft (black curve), and magnetic field vector (red curve). The spherical coordinates are displayed at 6000 temporal nodes for every sampled time

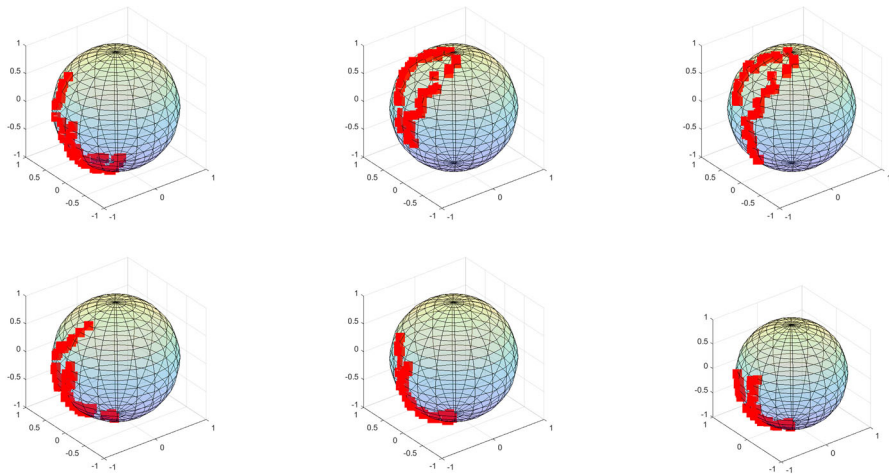


Fig. 21 Empirical intrinsic Fréchet curve mean of regressors (December, 1979–February, 1980 at the top, and March–May, 1980 at the bottom)

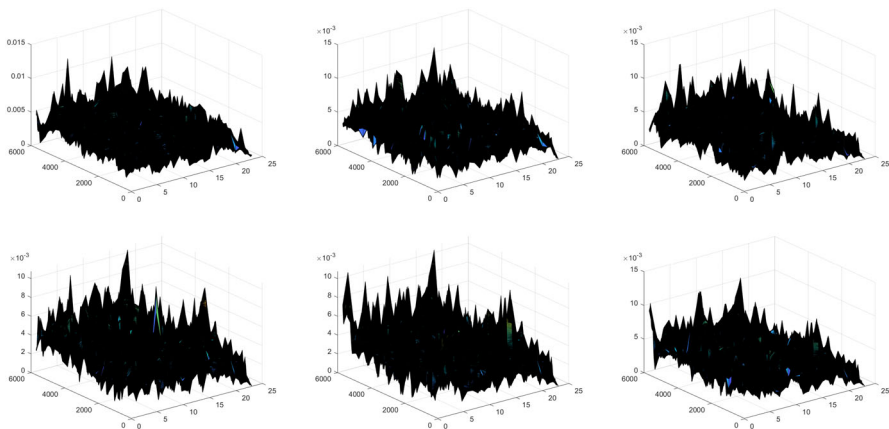


Fig. 22 Five fold cross validation quadratic angular functional errors (December, 1979–February, 1980 at the top, and March–May, 1980, at the bottom)

Acknowledgements Funding for open access charge: Universidad de Granada / CBUA. This work has been supported in part by projects MCIN/ AEI/PID2022-142900NB-I00, MCIN/ AEI/PGC2018-099549-B-I00, and CEX2020-001105-M MCIN/AEI/ 10.13039/501100011033).

Funding Funding for open access publishing: Universidad de Granada/CBUA.

Open Access This article is licensed under a Creative Commons Attribution 4.0 International License, which permits use, sharing, adaptation, distribution and reproduction in any medium or format, as long as you give appropriate credit to the original author(s) and the source, provide a link to the Creative Commons licence, and indicate if changes were made. The images or other third party material in this article are included in the article's Creative Commons licence, unless indicated otherwise in a credit line to the material. If material is not included in the article's Creative Commons licence and your intended use is not permitted by statutory regulation or exceeds the permitted use, you will need to obtain permission directly from the copyright holder. To view a copy of this licence, visit <http://creativecommons.org/licenses/by/4.0/>.

References

- Afsari B (2011) Riemannian L_p center of mass: existence, uniqueness, and convexity. *Proc Am Math Soc* 139:655–673
- Afsari B, Tron R, Vidal R (2013) On the convergence of gradient descent for finding the Riemannian center of mass. *SIAM J Control Optim* 51:2230–2260
- Bhattacharya A, Bhattacharya R (2012) *Nonparametric inference on manifolds: with applications to shape spaces*. Cambridge University Press, New York
- Buss SR, Fillmore JP (2001) Spherical averages and application to spherical splines and interpolation. *ACM Trans. Graph.* 20:95–126
- Chavel I (2006) *Riemannian Geometry*, 2nd edn. Cambridge Studies in Advanced Mathematics, vol 98. Cambridge University Press, Cambridge
- Chen D, Müller H-G (2012) Nonlinear manifold representations for functional data. *Ann Stat* 40:1–29
- Dai X, Müller H-G (2018) Principal component analysis for functional data on Riemannian manifolds and spheres. *Ann Stat* 46(6B):3334–3361
- Di Marzio M, Panzera A, Taylor CC (2014) Nonparametric regression for spherical data. *J Am Stat Assoc* 109:748–763
- Dimeglio Ch, Gallón S, Loubes J-M, Maza E (2014) A robust algorithm for template curve estimation based on manifold embedding. *Comput Stat Data Anal* 70:373–386
- Galeano P, Joseph E, Lillo RE (2015) The Mahalanobis distance for functional data with applications to classification. *Technometrics* 57:281–291
- Jammalamadaka RS, Terdik G (2022) Simulation and visualization of 3D-spherical distributions. In: Sen-Gupta A, Arnold BC (eds) *Directional statistics for innovative applications*. Springer, Singapore, pp 119–145
- Jupp PE, Kim PT, Koo JY, Wiegert P (2003) The intrinsic distribution and selection bias of long-period cometary orbits. *J Am Stat Assoc* 98:515–521
- Khardani S, Yao AF (2022) Nonparametric recursive regression estimation on Riemannian manifolds. *Stat Probab Lett* 82:109274
- Kim YT, Park HS (2013) Geometric structures arising from kernel density estimation on Riemannian manifolds. *J Multivar Anal* 114:112–126
- Kuelbs J (1970) Gaussian measures on a Banach space. *J Funct Anal* 5:354–367
- Lazar D, Lin L (2017) Scale and curvature effects in principal geodesic analysis. *J Multivar Anal* 153:64–82
- Le H, Barden D (2014) On the measure of the cut locus of a Fréchet mean. *Bull Lond Math Soc* 46:698–770
- Lin L, Thomas B, Zhu H, Dunson DB (2017) Extrinsic local regression on manifold-valued data. *J Am Stat Assoc* 112:1261–1273
- Lin Z, Yao F (2017) Functional regression with unknown manifold structures. [arXiv:1704.03005](https://arxiv.org/abs/1704.03005)
- Panaretos VM, Tavakoli S (2013) Fourier analysis of stationary time series in function space. *Ann Stat* 41:568–603
- Parthasarathy KR (1967) *Probability measures on metric spaces*. Academic Press, New York
- Patrangaru V, Ellingson L (2016) *Nonparametric statistics on manifolds and their applications to object data analysis*. Taylor & Francis Group, LLC, Boca Raton
- Pelletier B (2005) Kernel density estimation on Riemannian manifolds. *Stat Prob Lett* 73:297–304
- Pelletier B (2006) Non-parametric regression estimation on closed Riemannian manifolds. *J Nonparametr Stat* 18:57–67
- Petersen A, Müller H-G (2019) Fréchet regression for random objects with Euclidean predictors. *Ann Stat* 49:691–719
- Pigoli D, Menafoglio A, Secchi P (2016) Kriging prediction for manifold-valued random fields. *J Multivar Anal* 145:117–131
- Ruiz-Medina MD, Álvarez-Liéñana J (2019) Strongly consistent autoregressive predictors in abstract Banach spaces. *J Multivar Anal* 170:186–201
- Torres-Signes A, Frías MP, Ruiz-Medina MD (2021) COVID-19 mortality analysis from soft-data multivariate curve regression and machine learning. *Stoch Env Res Risk Assess* 35:2659–2678
- Van der Vaart AW, Wellner JA (1996) *Weak convergence and empirical processes. With applications to statistics*. Springer, New York
- Zhou H, Li L, Zhu H (2013) Tensor regression with applications in neuroimaging data analysis. *J Am Stat Assoc* 108:540–552
- Zhu H, Chen Y, Ibrahim JG, Li Y, Hall C, Lin W (2009) Intrinsic regression models for positive-definite matrices with applications to diffusion tensor imaging. *J Am Stat Assoc* 104:1203–1212

Publisher's Note Springer Nature remains neutral with regard to jurisdictional claims in published maps and institutional affiliations.